# TP53BP2 Promotes Placental Autophagy and Pre-eclampsia via G9a and DNMT1 Cooperatively Modulating E2F1

Nan Jiang[1], Qiujun Liu[2], Shaoying Wen[2], Pengzhi Yin[3], Wen Zeng[4], Jingyu Wang[1], Qingyun Song[1], Yinju Hao[2], Guizhong Li[2], Kai Wu[2], Yuhui Liao[5], Huiping Zhang[3], and Shengchao Ma[2]

[1]Central South University
[2]Ningxia Medical University
[3]Chinese University of Hong Kong
[4]Central Hospital of Shaoyang City
[5]Kunming Medical University

December 30, 2024

**Abstract**

Pre-eclampsia (PE) is a global pregnancy-related disorder that is characterized mainly by impaired migration and invasion of trophoblast cells. Recently, autophagy has been shown to play a vital role in PE. However, the precise regulatory mechanisms underlying the upregulation of autophagy are still unclear. In this study, TP53BP2 expression was significantly upregulated in trophoblasts. Silencing TP53BP2 not only decreases autophagy but also attenuates the progression of PE in rats. Moreover, TP53BP2 expression was positively correlated with systolic blood pressure, diastolic blood pressure and body mass index (BMI) but was negatively correlated with gestational age at delivery and neonatal birth weight. Furthermore, our findings suggest that TP53BP2 enhances autophagy in trophoblasts by promoting the release of Beclin-1 from the Bcl-2/Beclin-1 complex. Additionally, DNMT1 and G9a were found to downregulate TP53BP2 expression through a cooperative reduction in DNA methylation and H3K9me2 enrichment at the promoter region of TP53BP2. More importantly, cooperation between DNMT1 and G9a suppressed the binding of E2F1 at the TP53BP2 promoter, leading to transcriptional inhibition of TP53BP2 in PE trophoblasts. In conclusion, our findings suggest that TP53BP2 promotes autophagy in trophoblasts of preeclamptic placentas through DNA methylation and H3K9me2-mediated transcriptional regulation and may serve as a potential therapeutic target for early-onset PE.

## Introduction

Pre-eclampsia (**PE** ), which occurs in 3% to 7% of all pregnancies, is one of the leading causes of maternal and fetal morbidity and mortality worldwide1(). PE can be classified into two main types on the basis of the timing of its onset during pregnancy: early-onset and late-onset PE. Early-onset PE is a serious condition of pregnancy characterized by high blood pressure and often a significant amount of protein in the urine2(). It typically occurs before 34 weeks of gestation and cannot always be prevented3(). Insufficient trophoblast invasion, impaired uterine spiral artery remodeling, placental dysfunction, and endothelial dysfunction have been reported in early-onset PE pregnancies4(). Autophagy is a fundamental biological process in which cells degrade and recycle their own components. During early pregnancy, autophagy contributes to embryogenesis and is involved in the normal development of embryos56(,). Moreover, autophagy has been shown to accelerate trophoblast aging under conditions of oxygen deprivation, leading to exacerbated trophoblast dysfunction and deficiency7(). Clinical evidence has revealed that the pathophysiology of PE is related to increased LC3B-mediated autophagy8(). In addition, our previous study reported that autophagy is in-

creased both in placentas from PE pregnancies and in trophoblasts under hypoxia and that the inhibition of autophagy may serve as a promising approach for adjuvant chemotherapy for PE9(). However, the exact role of autophagy **in PE trophoblasts** is unclear, and the initial factors that trigger this process are still poorly understood.

The tumor suppressor p53-binding protein 2 (TP53BP2) is a gene that encodes a protein that plays a significant role in regulating apoptosis10()**. Endogenous TP53BP2** is damage inducible and modulates physiologic damage response pathways involved in diverse cellular functions11(). Recent studies have indicated that TP53BP2 is overexpressed in various tumor types and is a critical factor in tumorigenesis and development1213(,). In addition, TP53BP2 has a crucial influence on the proliferation and metastasis of triple-negative breast cancer cells, and the functional mechanism may be p53 independent to a great extent14(). Recent studies have shown that TP53BP2 can regulate autophagy through its N-terminal domain, which shares high structural similarity with ATG12 and LC313 because of the presence of the ubiquitin-fold sharing motif15(). Liu *et al* . reported that the overexpression of TP53BP2 inhibited autophagy at low-dose gp120 (a soluble envelope glycoprotein, 50 ng/mL) but induced autophagy at high-dose gp120 (200 ng/mL) in SH-SY5Y neuroblastoma cells; in turn, TP53BP2 knockdown attenuated the autophagy induced by high-dose gp12016(). These results suggested that TP53BP2 could regulate autophagy in diseases in a gp120 concentration-dependent manner. In addition, studies have shown that TP53BP2 inhibits RAS-induced autophagic activity to dictate the cellular response to RAS17(). Notably, many studies have shown that impaired trophoblast invasion and incomplete spiral artery remodeling are among the main causes of PE 1819(,). This observation of aberrant expression and the dual function of TP53BP2 led us to hypothesize that this molecule may be involved in the pathogenesis of PE through the regulation of autophagy.

**Abnormal DNA methylation during placentation is the most important epigenetic factor correlated with PE** 20(). Moreover, changes in histone modifications, such as acetylation, can also result in PE. Gene expression is regulated by various factors, such as the presence of DNA methylation marks or binding sites for transcription factors21(). Among histone modifications, histone methylation is a complex epigenetic mechanism that can activate or repress the transcription of target genes by altering the chromosomal structure, depending on the location of the methylation site22(). Interestingly, DNA methylation regulates gene expression by suppressing gene transcription. Similarly, it modifies the chromatin structure and interacts with other epigenetic modifications, thereby enabling more diverse regulation of gene expression2324(,). In mammals, the patterns of DNA methylation in somatic cells are determined mainly by the activity of DNMT125(). The direct interaction between DNMT1 and G9a is proposed to coordinate DNA methylation and H3K9 methylation during DNA replication26(). The transcription activity of a specific gene is known to be regulated by epigenetic markers and the interplay between transcription factors and the cis elements of specific promoters in a time- and space-dependent manner, which is intricately linked to gene expression27(). In addition, as a member of the E2F family, E2F1 is involved in regulating cell cycle progression, cell differentiation and DNA repair2829(,). Some evidence suggests that specific binding of E2F1 and/or E2F2 to CpG islands protects against de novo DNA methylation through nucleosome depletion30(). Moreover, increased expression of E2F1 and increased CpG hydroxy methylation of the E2F1 binding motif conjointly induce ESRP1 expression in breast cancer31()**. Reports suggest that searching for abnormal DNA methylation (hypo/hyper) could be a reasonable approach to discover new markers related to PE, aiming to predict and understand the development of PE** 32().

In this study, we discovered that TP53BP2 regulates autophagy and plays a crucial role in the development of early-onset PE. Mechanistically, the cooperation of G9a and DNMT1 suppresses the binding of E2F1 to the TP53BP2 promoter, leading to decreased TP53BP2 expression and autophagy in PE trophoblasts, providing a possible new theoretical basis for targeted therapy for early-onset PE.

## Materials and Methods

### Patients and study samples

**Eighty-five placentas were obtained from women who underwent cesarean delivery at the Gen-**

**eral Hospital of Ningxia Medical University between 2017 and 2021.** PE was defined as a systolic blood pressure [?]140 mmHg and a diastolic blood pressure [?]90 mmHg in two consecutive measurements taken at least 6 h apart, along with proteinuria ([?]0.3 g/24 h) after 20 weeks of gestation. Placentas from non-PE pregnancy volunteers (pregnant controls (PCs), n=40), with no medical history or medication usage, served as controls.**Placentas in the PE pregnancy group (n=45) were obtained from pregnant patients who delivered with early-onset PE (<34 weeks gestation).** The exclusion criteria included multiple gestations, fetal congenital malformations/chromosomal abnormalities, recent infection, antiphospholipid antibodies, trauma, drug/alcohol abuse during pregnancy, hypertension that had been discovered before 20 weeks, thrombophilia with a history of PE, receiving anticoagulant/antiaggregation therapy, smoking, **and incomplete data from pregnant women's obstetric examinations. Placentas were collected from the central part within 10 min of cesarean delivery, avoiding macroscopic areas of infarction and calcification. After rinsing briefly in saline, the samples were frozen at -80°C or fixed in polyformaldehyde until further analyses. All experiments were conducted following the protocol approved by the Clinical Research Ethics Committee of Ningxia Medical University (NO. 2017-083), and informed consent was obtained from all patients.**

### Animal experiments

**All the animal experiments were performed in Sprague-Dawley (SD) rats (aged 13 –14 weeks) housed at Ningxia Medical University Laboratory Animal Center (Yinchuan, China). These rats were housed in a temperature-controlled room (22–24degC) with a 12-h light/dark cycle and had free access to food and water. Following a week of acclimatization, they were mated with healthy male SD rats at a 2:1 ratio. The onset of gestation was identified by the presence of vaginal sperm plugs on gestational day 1. The most reliable animal model of PE is the surgically induced reduced uterine perfusion pressure (RUPP) model. This model has been shown to induce hypertension, proteinuria, renal dysfunction, an antiangiogenic state, inflammation, oxidative stress, cardiac dysfunction and intrauterine growth restriction (IUGR), similar to PE in humans. Thus, on the 14th day of gestation, the rats underwent surgical RUPP under pentobarbital anesthesia. Briefly, through a midline incision, the abdominal cavity was opened to expose the lower abdominal aorta. Silver clips (0.203 mm) are placed around the aorta above the iliac bifurcation to the RUPP by approximately 40%. Simultaneously, silver clips (0.100 mm) are used to decrease the degree of ovarian collateral circulation of the bilateral uterine arteries at the ovarian ends of the uterine arch. The sham group underwent the same procedure as the RUPP group but without clip placement.** Recombinant adeno-associated virus (AAV) serotype 9 vectors carrying TP53BP2 short hairpin RNA (shRNA) (AAV-shTP53BP2), recombinant AAV serotype 9 vectors carrying DNMT1 shRNA (AAV-DNMT1), recombinant AAV serotype 9 vectors carrying G9a shRNA (AAV-shG9a), or recombinant AAV9 vectors carrying a negative control (AAV-shNC) were manufactured by GeneChem (Shanghai, China). Ten microlitres of virus (1.5E+11) **was injected into the placenta. On the 20th day of gestation, the rats were euthanized with pentobarbital, and the pups were removed and weighed. The placentas were washed with ice-cold physiological salt solution and preserved at -80degC for subsequent analysis. The animal experiments were approved by the Committee on the Ethics of Animal Experiments of Ningxia Medical University (NO. 2021–250).**

### Cell culture and treatment

Human trophoblast cell lines (HTR-8/SVneo and JEG-3 cells) were acquired from Fudan IBS Cell Center (China). These cells were maintained in either RPMI-1640 or Ham's F-12 medium enriched with 10% fetal bovine serum (FBS) and an antibiotic-antimycotic cocktail (100 U/mL penicillin (Solarbio, China) or 100 mg/mL streptomycin (Solarbio, China)) under a 5% $CO_2$ humidified atmosphere at 37degC. To simulate severe hypoxic conditions, the cells were plated at a density of 60 mm. After a 24-h period, they were placed in a NAPCO Series 8000WJ incubator (Thermo Fisher Scientific, USA) under 1% $O_2$ and 5% $CO_2$ at 37degC for 48 h. HEK293T cells were cultured

**in Dulbecco's modified Eagle's medium (DMEM) supplemented with 10% FBS, 100 U/mL penicillin and 100 mg/mL streptomycin. For the transfection experiments, the cells were subjected to viral infection with recombinant adenoviruses encoding TP53BP2 (Ad-TP53BP2), adenoviruses encoding DNMT1 (Ad-DNMT1), adenoviruses encoding G9a (Ad-E2F1), and adenoviruses encoding G9a (Ad-G9a), and adenoviruses encoding green fluorescent protein were used as a negative control (Ad-NC). Following a 4-hour incubation, the culture medium was replaced with regular RPMI-1640 supplemented with 7% FBS, and the cells were then exposed to hypoxic conditions at 37degC with 5% $CO_2$for 48 h. Additionally, these two cell lines were transfected with lentiviruses carrying sh-TP53BP2, sh-Beclin-1, sh-DNMT1, sh-E2F1, or sh-G9a, and sh-NC via Lipofectamine 2000 (Thermo Fisher Scientific, USA) following the manufacturer's protocol. After 6 h of incubation, the cells were cultured in 7% fetal bovine serum under hypoxic conditions at 37degC with 5% $CO_2$ for 48 h.**

**RNA-sequencing (RNA-seq) assay**

Total RNA was extracted from placental tissues to construct cDNA libraries. For the small RNA cDNA library, the complete RNA was first ligated with both an RNA 3' adapter and a 5' adapter. Subsequently, reverse transcription primers were used to convert the ligated RNAs into cDNAs. The resulting cDNAs were then amplified through polymerase chain reaction (PCR) and purified via gel electrophoresis. The quality of the cDNAs was assessed via an Agilent 2100 chip (Agilent, Santa Clara, USA). For the analysis of the RNA-seq library, the total RNA was purified to eliminate rRNA with the Ribo-Zero rRNA Removal Kit (Epicenter-Illumina, Madison, USA), followed by fragmentation of the RNA. The fragmented RNA was then converted into first-strand cDNA via a TruSeq(r) Stranded Kit (Epicenter-Illumina, Madison, USA). Double-stranded cDNA was generated via DNA polymerase I and RNase H. The 3' ends of the double-stranded cDNA were adenylated and then ligated with adapters. PCR amplification and purification were carried out to construct the cDNA library. The libraries were sequenced via the Illumina HiSeq 2500 platform for total RNA sequencing, which employs a 90-bp paired-end sequencing strategy, whereas small RNA sequencing was performed via the Illumina HiSeq X Ten platform.

**Transmission electron microscopy (TEM)**

The placentas were cut into approximately 1x1x1 mm pieces. HTR-8/SVneo and JEG-3 cells were washed with ice-cold PBS, digested with trypsin, and then collected via centrifugation. Both tissues and cells were subsequently fixed via a fixative buffer comprising 2% paraformaldehyde and 2.5% glutaraldehyde in 0.1 M phosphate buffer. Postfixation, the samples were embedded and sectioned at a thickness of 0.12 μm and then stained with uranyl acetate solution and lead citrate solution. Visualization of the ultrathin sections was accomplished through a JEOL transmission electron microscope (Zeiss, Germany).

**Immunofluorescence staining**

**Frozen sections of human and rat placentas were fixed in 4% paraformaldehyde for 15 min, followed by permeabilization with 0.2% Triton X-100 for 15 min. After blocking with 10% goat serum, the sections were incubated overnight at 4°C with the following primary antibodies: TP53BP2 (1:500, Abcam, Cambridge, USA), E2F1 (1:100, Abcam, Cambridge, USA), G9a (1:500, Abcam, Cambridge, USA), DNMT1 (1:500, Abcam, Cambridge, USA), H3K9me2 (1:500, Abcam, Cambridge, USA), and CK-7 (1:50, Abcam, Cambridge, USA). The sections were subsequently washed three times with PBS and incubated with fluorescein-conjugated secondary antibodies (1:500, Abcam, Cambridge, USA) for 1 h at 37°C. To visualize the cell nuclei, the sections were stained with 4,6-diamidino-2-phenylindole (DAPI). The fluorescence was observed and imaged via laser confocal microscopy (Zeiss, Jena, Germany).**

**Immunohistochemistry (IHC)**

The human and rat **placental tissue sections were deparaffinized in xylene and rehydrated through a graded series of ethanol solutions. Antigen retrieval was performed by immersing the sections**

**in 10 mM citrate buffer (pH 6.0) and heating them in a pressure cooker for 15 min. Endogenous peroxidase activity was quenched by incubating the sections in 3% hydrogen peroxide solution for 10 min. Subsequently, the sections were blocked with 5% inactivated goat serum for 1 h at room temperature. The sections were then incubated overnight at 4°C with the following primary antibodies: TP53BP2 (1:5** 00, Abcam, Cambridge, USA), LC3B (1:200, Abcam, Cambridge, USA), and p62 (1:200, Abcam, Cambridge, USA). After being washed with PBS, the sections were incubated with the secondary antibody for 2 h at room temperature. Immunoreactivity was visualized by the addition of 3,3'-diaminobenzidine (DAB) substrate solution. The sections were counterstained with Harris hematoxylin for 30 s to visualize the cell nuclei. Finally, the sections were dehydrated through ethanol and xylene, and images were captured via an optical microscope.

**Autophagic flux assay**

GFP-RFP-LC3 adenoviruses (HANBIO, Shanghai, China) were utilized to monitor autophagic flux. Briefly, when the cells reached 60% confluence, GFP-RFP-LC3 adenoviruses were added to the culture medium. After 8 h of adenoviral infection, the culture medium was replaced, and the cells were further incubated for 24 h. Subsequently, the cells were fixed with 4% formaldehyde for 10 min. Fluorescence images were captured via a laser confocal microscope (Zeiss, Jena, Germany). Typically, an increased number of red puncta (representing autophagic lysosomes) compared with yellow puncta (formed by the overlap of red and green) indicates activated autophagy, whereas a greater number of yellow puncta relative to red puncta suggests autophagy suppression.

**Western blot**

The tissue and cells were lysed in ice-cold lysis buffer (KeyGEN Biotech, Nanjing, China) followed by centrifugation at 4°C for 15 min. Cell lysates were separated by 8% SDS-PAGE and then transferred to polyvinylidene difluoride (PVDF) membranes (Millipore, Billerica, USA). After blocking with 5% nonfat milk, the membranes were incubated overnight at 4degC with specific primary antibodies against the following proteins: TP53BP2 (1:1000, Abcam, Cambridge, USA), LC3B (1:1000, Abcam, Cambridge, USA), p62 (1:1000, Abcam, Cambridge, USA), Beclin-1 (1:1000, Abcam, Cambridge, USA), Bcl-2 (1:1000, Abcam, Cambridge, USA), E2F1 (1:1000, Abcam, Cambridge, USA), DNMT1 (1:1000, Abcam, Cambridge, USA), and G9a (1:1000, Abcam, Cambridge, USA). After three washes, the membranes were incubated with horseradish peroxidase (HRP)-conjugated secondary antibodies for 1 h, after which protein expression was detected via a chemiluminescence kit (KeyGEN, Nanjing, China). The optical density of each band was analyzed via densitometry and normalized to that of a β-actin loading control.

**Quantitative real-time polymerase chain reaction (qRT-PCR) analysis**

**Total RNA was isolated from human placentas and cells** via an RNA isolation kit (TIANGEN, Beijing, China) following the manufacturer's instructions. **Following quantification of the RNA, cDNA was synthesized via a reverse transcription kit (Takara, Tokyo, Japan). The cDNA was subsequently subjected to real-time PCR amplification in a thermal cycler via TBGreen Fast qPCR mix (Takara, Tokyo, Japan). All experiments were performed in triplicate, and the data were normalized to those of GAPDH. The specific primer sequences are provided in Table S1.**

**Methylation-specific PCR (MSP) assays**

**MSP assays were performed to assess the DNA methylation status. Briefly,** genomic DNA was extracted from placentas and HTR-8/SVneo cells via DNA extraction kits (TIANGEN, Beijing, China) following the manufacturer's instructions. The bisulfite conversion of DNA was carried out via EZ DNA methylation Gold (ZYMO Research Corporation, USA). Methylation-specific primers were subsequently designed to selectively amplify either methylated or unmethylated DNA sequences of the TP53BP2 promoter region. After amplification, the PCR products were analyzed via 2% **gel electrophoresis to visualize the presence or absence of specific bands corresponding to methylated or unmethylated DNA, respectively. The primer sequences for the MSP assays are provided in Table S2.**

### Bisulfite-sequencing PCR (BSP)

The DNA from the MSP results was subjected to sodium bisulfite treatment via a DNA bisulfite kit (Qiagen, Beijing, China) according to the manufacturer's instructions. After bisulfite conversion, the DNA was purified and recovered via the SanPrep Column DNA Gel Extraction Kit (Sangon, Shanghai, China). Primers for bisulfite pyrosequencing were designed to target the specific region of interest and were utilized with 3730 sequencing analyzers. The primers for the TP53BP2 methylation reaction were as follows: TP53BP2 forward: 5'-AACTTCACGGTGGGTTTCAAGC-3'; TP53BP2 reverse: 5'-GTGCAGGCCTGAGCCTTCT GGC-3'.

### Coimmunoprecipitation (Co-IP)

The cells were washed three times with PBS and subsequently lysed on ice in lysis buffer (Beyotime, Beijing, China). Next, the lysates were centrifuged at 12,000 × g for 15 min. Subsequently, the cell lysates were incubated with specific antibodies for 1 h, followed by a 30-minute incubation with Dynabeads Protein G beads at 4degC. The beads were then washed three times with cold lysis buffer. Following the washes, the beads were boiled in 10 μL of 5× loading buffer (Beyotime, Shanghai, China) for 5 min before being analyzed by western blot using antibodies against DNMT1, G9a, E2F1, Flag, Myc, and GST.

### Chromatin immunoprecipitation (ChIP) assay

**ChIP assays were conducted following the manufacturer's instructions (Millipore). Antibodies against H3K4me1, H3K4me2, H3K4me3, H3K9me2, H3K9me3, H3K36me3, H3K27me3, G9a, DNMT1 or E2F1 were utilized for ChIP. RT-PCR was performed with specifically designed qPCR primers targeting the proximal promoter region of TP53BP2. IgG was used as a negative control to measure nonspecific background signals via immunoprecipitation. The resulting amplified product was evaluated through electrophoresis, and the signals were quantified as a percentage of the input. The primer sequences are provided in Table S3.**

### Luciferase reporter assay

A luciferase reporter assay was conducted to assess the activity of the TP53BP2 promoter. For the promoter activity assay, various fragments of the TP53BP2 promoter (-35/+1, -599/+1, -1018/+1, -1530/+1, -599/+641, and -2000/+1) were inserted into the pGL3-Basic plasmid. The cells were then seeded in 24-well plates and cotransfected with the aforementioned reporter constructs and a Renilla luciferase reporter plasmid. Following a 48-hour transfection period, the luciferase activities were quantified via a dual-luciferase reporter assay system (Promega, Madison, USA). The firefly luciferase activity was determined and normalized to the Renilla luciferase activity. The reported data represent the average of three independent experiments.

### Statistical analysis

The data from three replicates per experiment are summarized as mean ± SD. The statistical analysis involved one-way ANOVA, followed by the Student-Newman-Keuls' test for multiple comparisons within treatment groups or Student's $t$ test for comparisons between two groups. ROC curves and the corresponding area under the curve (AUC) were generated via the R package "pROC" to assess the diagnostic value of TP53BP2. A significance threshold of $P$ <0.05 was applied.

## Results

### Identification and validation of TP53BP2 in placental

### trophoblasts in PE

To elucidate the molecular mechanisms underlying the autophagy of placental trophoblasts in early-onset PE, we employed RNA-seq **to examine autophagy-related differentially expressed genes (DEGs) in placentas derived from early-onset** PE pregnancies compared with those from non-PE pregnancies. The functionally related genes were enriched predominantly in autophagy-related signaling pathways,

such as the PI3K-Akt signaling, AMPK signaling, and mTOR signaling pathways (**Figure 1A** ). The cluster heatmaps show the top 20 DEGs involved in autophagy-related signaling pathways in placentas from PE pregnancies (**Figure 1B** ). Among them, TP53BP2 was the most robust inducer (**Figure 1C** ). Moreover, TP53BP2 expression was markedly greater in placentas from PE pregnancies than in those from non-PE pregnancies(**Figure 1D** ). Immunohistochemical and immunofluorescence staining further revealed the upregulation of TP53BP2 in trophoblasts from PE pregnancies (**Figure 1E, F)** . To investigate the functional role of TP53BP2, we conducted TP53BP2 overexpression and knockdown in HTR8/Svneo and JEG-3 cells by transfecting Ad-TP53BP2 or three independent sh-TP53BP2 vectors, respectively (**Figure S1** ). TEM revealed increased autophagosome and autolysosome formation in trophoblasts transfected with Ad-TP53BP2, whereas the opposite effect was observed in those transfected with sh-TP53BP2 (**Figure 1G** ). Additionally, an autophagic flux assay using tandem fluorescent GFP-RFP-LC3 revealed a decrease in total autophagosome and autolysosome formation in trophoblasts transfected with sh-TP53BP2 **(Figure 1H** ). LC3B-II and p62 serve as complementary markers of autophagy, with LC3B-II reflecting autophagosome formation and p62 indicating the process of substrate recognition and degradation. Therefore, the protein expression of LC3B-II and p62 was assayed to determine the extent of autophagy. The results of the western blot analysis confirmed the effect of TP53BP2 on the LC3B-II and p62 levels in HTR8/SVneo and JEG-3 cells under hypoxia (**Figure 1I** ). These results demonstrated that the upregulation of TP53BP2 could increase trophoblast autophagy in PE placentas.

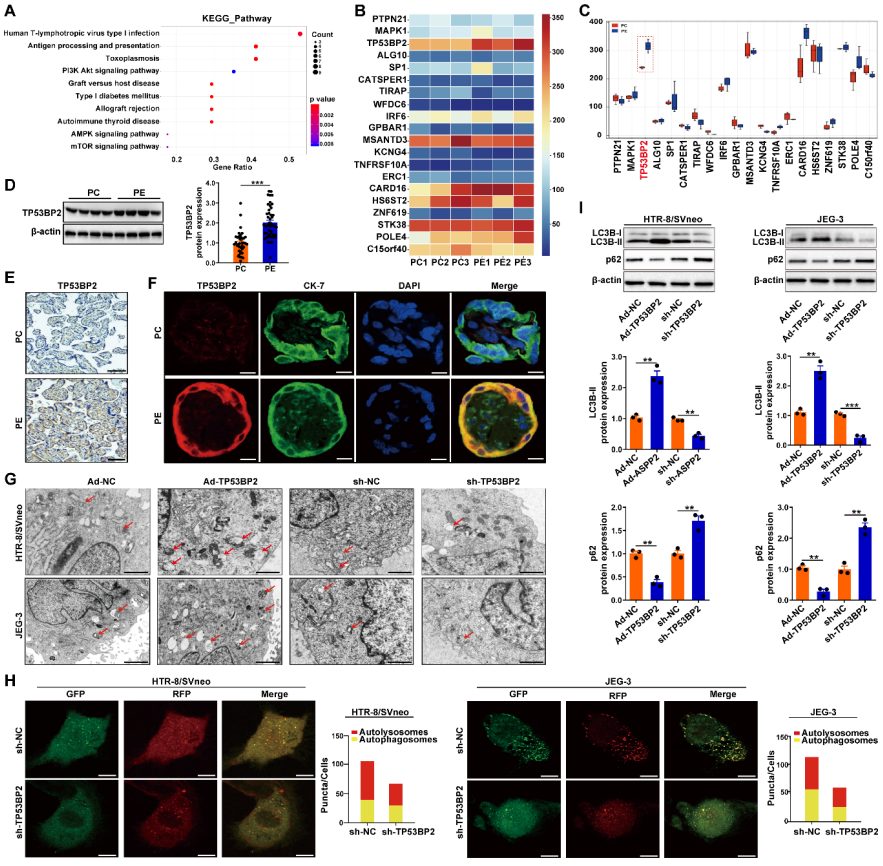


**Figure 1. TP53BP2 was upregulated in placental trophoblasts from PE pregnancies. (A) KEGG signaling pathway histogram. (B) Cluster heatmap showing the top 20 autophagy-related** DEGs associated with autophagy (|fold change|[?]2.0,$P$ [?]0.05) in placentas from PE pregnancies and non-PE pregnancies. The red and blue strips indicate upregulated and downregulated genes, respec-

tively. **(C) Box plot** illustrating **the expression of** the top 20 DEGs in placentas from PE pregnancies and non-PE pregnancies. The blue box plot represents PE pregnancies, and the red box plot represents non-PE pregnancies. **(D)** The expression of TP53BP2 in placentas was detected via western blotting (**PC, n=40; PE, n=45** ). **(E)** Representative immunohistochemical staining of TP53BP2. Scale bar=200 μm. **(F)** Double immunofluorescence staining showing colocalization of TP53BP2 (red) and CK-7 (trophoblast marker, green). Nuclei were stained with DAPI (blue). Scale bar=50 μm. **(G)** Autophagosomes in HTR8/Svneo and JEG-3 cells transfected with Ad-TP53BP2 or sh-TP53BP2 under hypoxia were observed via transmission electron microscopy (TEM). Scale bar=1000 nm.**(H)** Representative images of GFP-RFP-LC3 staining in HTR8/Svneo and JEG-3 cells transfected with sh-TP53BP2 under hypoxia (**n=** 3). Scale bar=20 μm. **(I)** The expression of LC3B-II and p62 in HTR8/Svneo and JEG-3 cells transfected with Ad-TP53BP2 or sh-TP53BP2 under hypoxia was detected by western blotting (**n=** 3). The data are presented as the means ± SDs.$^{**}P$ <0.01,$^{***}P$ <0.001.

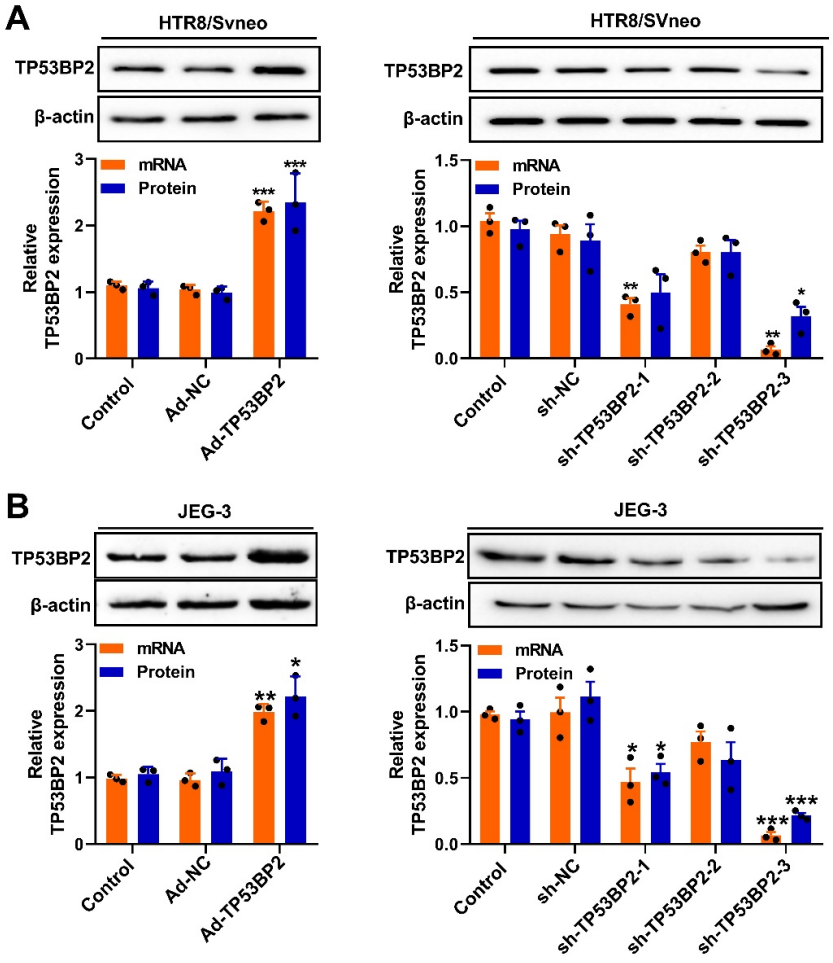


**Fig ure S1. Expression of TP53BP2 in HTR8/SVneo and JEG-3 cells. (A, B)** The expression of TP53BP2 in HTR8/SVneo and JEG-3 cells transfected with Ad-TP53BP2 or sh-TP53BP2 was examined via qRT-PCR and western blotting. The data are presented as the means ± SDs.$^{*}P$ <0.05,$^{**}P$ <0.01,$^{***}P$ <0.001.

**TP53BP2 silencing attenuates PE progression by reducing autophagy in rats**

On the basis of these in vitro findings, we established a PE model by inducing RUPP in rats on the 14th day of gestation to investigate the role of TP53BP2 (**Figure 2A-D** ). Knockdown of TP53BP2 via the use of recombinant adeno-associated virus serotype 9 vectors carrying TP53BP2 shRNA (AAV-shTP53BP2) in PE rats resulted in decreased blood pressure (**Figure 2E** ) and **proteinuria (Figure 2F** ) and increased fetal weight **(Figure 2G** ). HE staining also revealed a reduction in both hydropic degeneration of decidual cells and deposition of fibrous proteins in this rat model **(Figure 2H** ). Furthermore, placentas from preeclamptic rats with downregulated TP53BP2 presented reduced LC3B-II expression and increased p62 expression (**Fig 2I). Similar results were observed by immunofluorescence staining (Figure 2J** ). Additionally, immunohistochemical staining revealed a significant reduction in LC3B expression and upregulation of p62 expression **in placentas from preeclamptic rats subjected to TP53BP2 knockdown (Figure 2K** ). Collectively, these results suggest that TP53BP2 knockdown attenuated autophagy in trophoblasts in the placenta of preeclamptic rats.

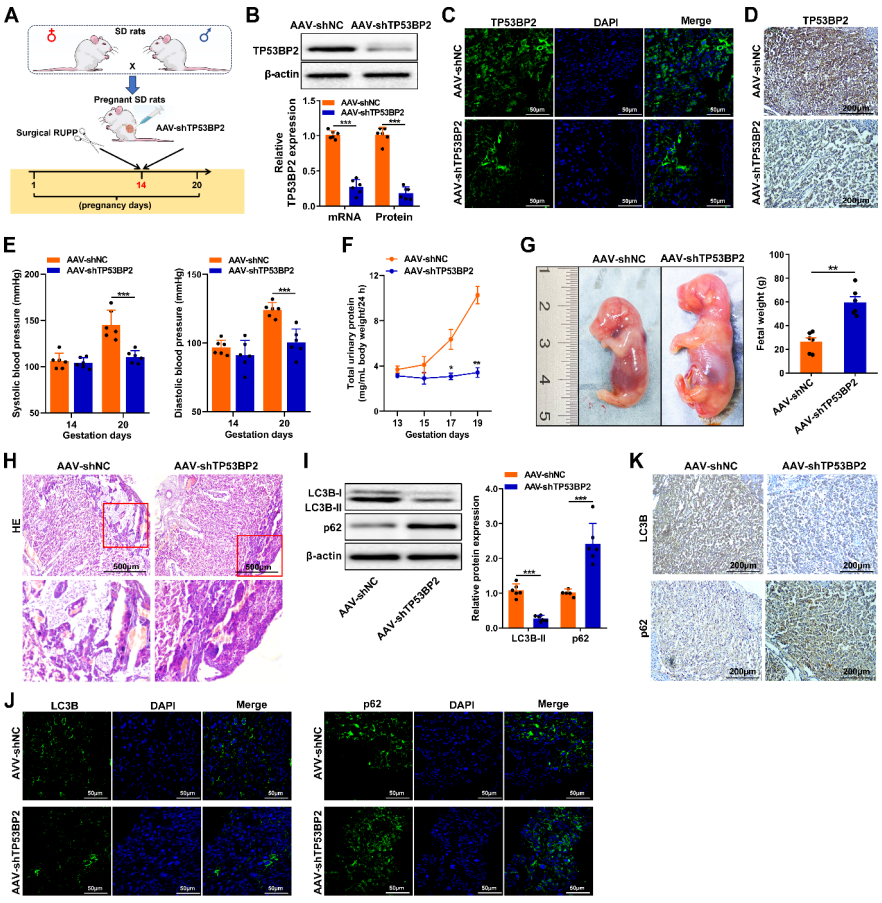


**Figure 2. TP53BP2 is a potential therapeutic target for the autophagy of trophoblasts in PE.** **(A)** On gestational day 14, SD rats underwent surgical reduction of uterine perfusion pressure (RUPP), followed by a single injection of 10 μL of AAV-shTP53BP2 (1.5E+11) into the placenta. **(B)** The expression of TP53BP2 in placentas from preeclamptic rats was detected by western blot and qRT-PCR. **(˚) Ιμμυνο-φλυορεσσενσε σταινινγ σηοωινγ ΤΠ53ΒΠ2 εξπρεσσιον ιν πλαχεντας φρομ πρεεχλαμπτις ρατς. Σχαλε βαρ=50 μμ. (Δ)** Immunohistochemical staining was used to detect the expression of TP53BP2 in placentas from preeclamptic rats. Scale bar=200 μm. **(E)** Systolic and diastolic blood pressure were measured via a noninvasive tail-cuff blood pressure measurement system in preeclamptic rats. **(F)** Total urine protein levels were measured via a protein assay in preeclamptic rats.**(G)** Gross appearance and

birthweight of the fetus at embryonic day 18.5 (E18.5). **(H)** HE staining analysis of placental pathological changes in preeclamptic rats. Scale bar=500 μm.**(I)** The expression of LC3B-II and p62 in placentas from preeclamptic rats was detected by western blot. **(J)** Immunofluorescence staining was used to detect the expression of LC3B and p62 in placentas from preeclamptic rats. Scale bar=50 μm.**(K)** Immunohistochemical staining was used to detect the expression of LC3B and p62 in placentas from preeclamptic rats. Scale bar=200 μm. The data are presented as the means ± SDs.$^{*}P$ <0.05,$^{**}P$ <0.01,$^{***}P$ <0.001.

**TP53BP2 enhances trophoblast autophagy by regulating Beclin-1 expression**

Next, we performed RNA-seq on HTR8/SVneo cells with TP53BP2 knockdown to investigate the molecules involved in autophagy. The results revealed the upregulation of 1046 molecules and the downregulation of 1035 molecules (|fold change|[?]2.0, $P$ [?]0.05) (**Figure 3A** ). GO analysis revealed that these molecules are involved in **autophagy, ATP binding, protein serine/threonine kinase activity, mTOR signaling, the HIF1 signaling pathway and AMPK signaling (Figure S2** ). A qRT-PCR assay was subsequently employed to measure the levels of the top 10 downregulated genes. The results revealed a significant reduction in the level of Beclin-1, a key marker of **autophagy,** in the placentas of preeclamptic rats (**Figure 3B, C** ). To further confirm the role of Beclin-1 in TP53BP2-induced autophagy, sh-Beclin-1 and Ad-TP53BP2 were cotransfected into HTR8/SVneo or JEG-3 cells **under hypoxia (Figure S3).** As shown in **Figure 3D** , cotransfection with sh-Beclin-1 and Ad-TP53BP2 resulted in a decrease in LC3B-II levels and an increase in p62 expression in both HTR8/SVneo and JEG-3 cells. Bcl-2 is known to interact with Beclin-1, an initiator of autophagy. Previous results indicate that the release of Beclin-1 from the Bcl-2–Beclin-1 complex then initiates TP53BP2-induced autophagy. Here, we investigated the role of Bcl-2 binding to the BH3 domain of Beclin-1 in TP53BP2-induced autophagy in trophoblasts. Coimmunoprecipitation (co-IP) revealed an increase in the interaction between TP53BP2 and Bcl-2, whereas disruption of the interaction between Beclin-1 and Bcl-2 was observed in HTR8/SVneo and JEG-3 cells under hypoxia **(Figure 3E** ). Conversely, knockdown of TP53BP2 increased the interaction between Beclin-1 and Bcl-2 **(Figure 3F** ). Taken together, these results demonstrate that knockdown of TP53BP2 inhibits trophoblast autophagy by decreasing Beclin-1 expression and promoting the interaction between Beclin-1 and Bcl-2.

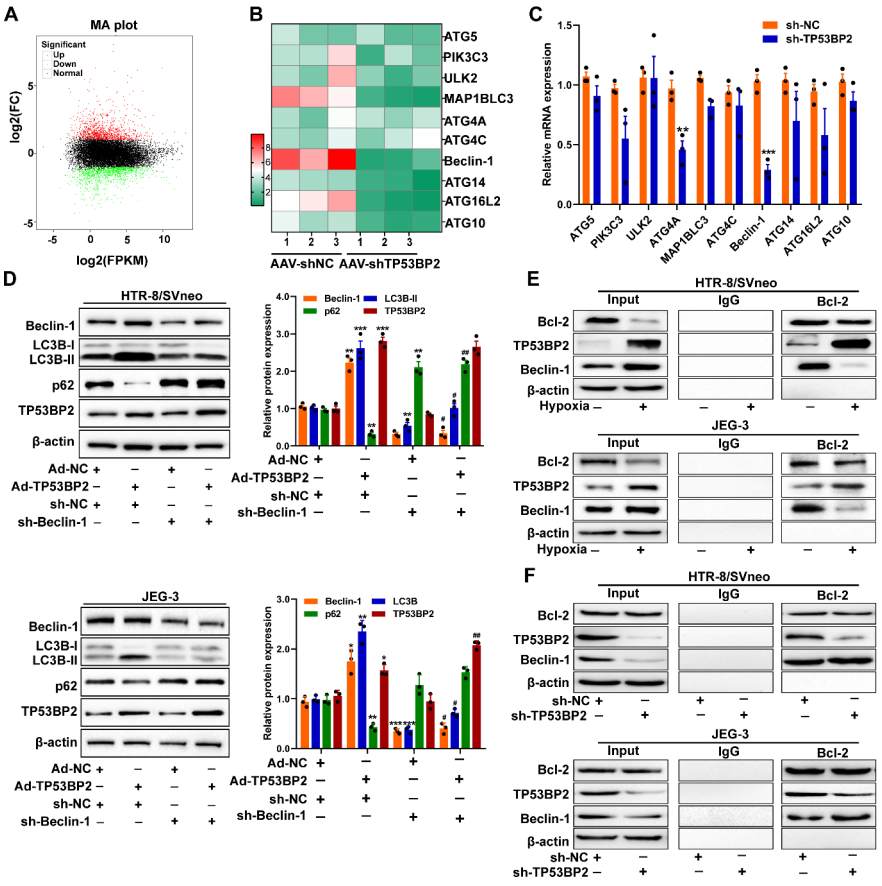


**Figure 3. TP53BP2 enhances trophoblast autophagy by regulating Beclin-1 expression. (A)** Volcano plot of 2081 DEGs in HTR8/SVneo cells transfected with sh-TP53BP2. The red dots and green dots indicate upregulated and downregulated gene expression, respectively (|fold change|[?]2.0, $P$ [?]0.05), and the black dots indicate unchanged genes. **(B) Heatmap of the top 10 downregulated autophagy-related genes in placentas from preeclamptic rats injected with AAV-shTP53BP2** . **(C) qRT-PCR validation of the top 10 downregulated genes. (D)** The expression of Beclin-1, LC3B-II, p62 and TP53BP2 in HTR8/SVneo and JEG-3 cells transfected with Ad-TP53BP2 and/or sh-Beclin-1 under hypoxia was detected by western blotting. (E) Coimmunoprecipitation (co-IP) assay followed by immunoblotting showing the interactions of Bcl-2 with TP53BP2 and Beclin-1 in HTR8/SVneo and JEG-3 cells under hypoxia. The cell lysates were subjected to immunoprecipitation with an anti-Bcl-2 antibody.**(F)** Co-IP assay followed by immunoblotting showing the interactions of Bcl-2 with TP53BP2 and Beclin-1 in HTR8/SVneo and JEG-3 cells transfected with sh-TP53BP2 under hypoxia. The data are presented as the means ± SDs. $^{*}P$ <0.05,$^{**}P$ <0.01,$^{***}P$ <0.001;$^{\#}P$ <0.05,$^{\#\#}P$ <0.01.

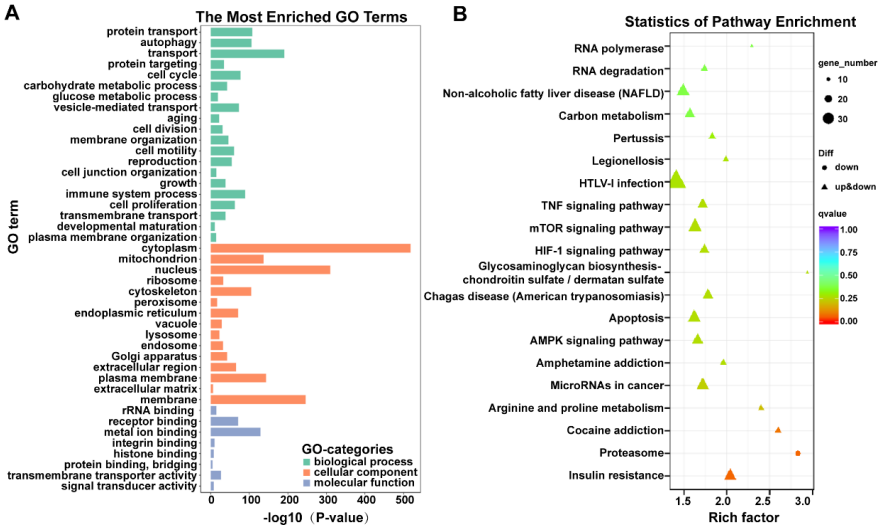


**Figure S2. GO and KEGG enrichment analyses of DEGs in trophoblasts transfected with sh-TP53BP2. (A) Histogram of the results of the Gene Ontology (GO) enrichment analysis of the DEGs. The GO terms included biological processes, molecular functions, and cellular components. The vertical axis represents the GO annotation; the horizontal axis represents the number of genes. (B)** Scatter plot of the results of the KEGG enrichment analysis of DEGs.

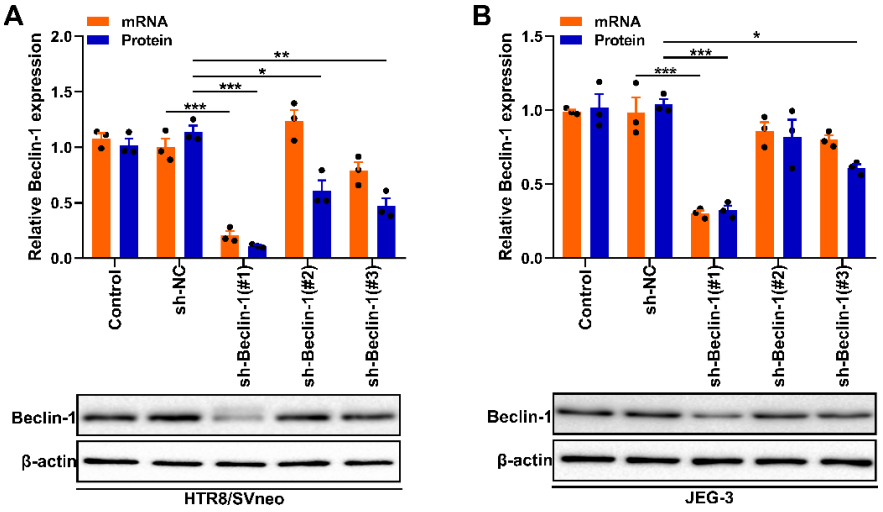


**Figure S3. Expression of Beclin-1 in HTR8/SVneo and JEG-3 cells. (A, B)** The expression of Beclin-1 in HTR8/SVneo and JEG-3 cells transfected with three sh-Beclin-1 or sh-NC strains was examined via qRT-PCR and western blotting. The data are presented as the means ± SDs.$^{*}P$ <0.05,$^{**}P$ <0.01,$^{***}P$ <0.001.

**TP53BP2 is associated with the clinicopathological characteristics of PE**

**To explore the clinical significance of TP53BP2 in the progression of PE, we collected 85 placentas from early-onset PE pregnancies (<34 weeks of gestation, n=45) and non-PE pregnancies (n=40). The pathological characteristics of these pregnancies are presented in Table 1. There was no significant difference in maternal age or fetal sex between PE pregnancies**

**and non-PE pregnancies ($P>0.05$). However, systolic and diastolic blood pressure, as well as proteinuria, were significantly increased in PE pregnancies ($P<0.0001$). Additionally, there was a significant difference in maternal body mass index (BMI) between PE pregnancies and non-PE pregnancies ($P<0.05$). Moreover, compared with non-PE pregnancies, PE pregnancies were associated with decreased gestational age at delivery and lower neonatal birth weight ($P<0.05$), indicating that these clinicopathological parameters were in accordance with the diagnostic criteria. To evaluate the significance of TP53BP2 in placental dysfunction, we analyzed the correlation between TP53BP2 and LC3B-II and p62 in placentas. The results revealed a positive association between TP53BP2 levels and LC3B-II levels in both PE and non-PE pregnancies but a negative correlation with p62 (Figure 4A, B). Additionally, TP53BP2 levels in placentas were positively correlated with systolic blood pressure, diastolic blood pressure, and BMI but negatively correlated with gestational age at delivery and neonatal birth weight (Figure 4C-G** ). Furthermore, receiver operating characteristic (ROC) analysis demonstrated that TP53BP2 had the highest area under the curve (AUC) value of 0.882 for diagnosing PE pregnancies (**Figure 4H). Taken together, these results suggest that TP53BP2 could serve as a predictive biomarker associated with the clinicopathological characteristics of PE pregnancies.**

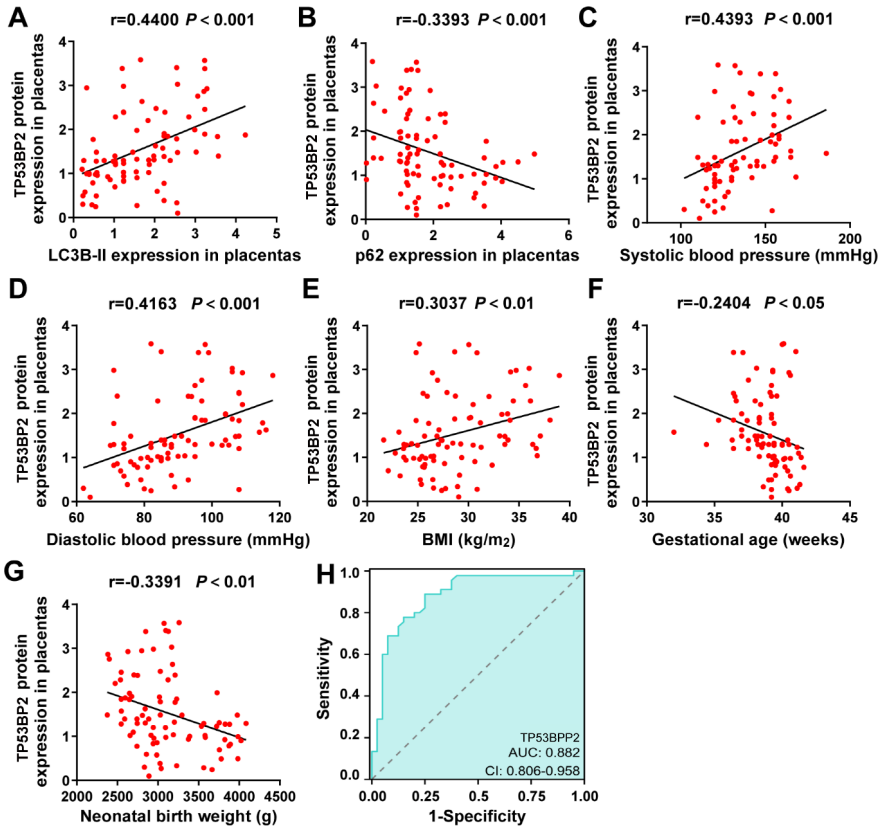


**Figure 4. Correlations between TP53BP2 and the clinicopathological characteristics of patients with PE. (A, B)** Pearson's correlation analysis between TP53BP2 expression and LC3B-II or p62 in placentas from PE pregnancies and non-PE pregnancies.**(C-G)** Pearson's correlation analysis between TP53BP2 expression and systolic blood pressure **(C)** , diastolic blood pressure**(D)** , BMI **(E)** , gestational age **(F)** , and neonatal birth weight **(G)** in PE pregnancies and non-PE pregnancies. **(H)** The cutoff value, sensitivity, and specificity were established via receiver operating characteristic (ROC) curves to evaluate the diagnostic value of TP53BP2 in PE pregnancies. The data are presented as the means ± SDs. $^{**}P$ <0.01.

**Table 1. Clinical data of non-PE pregnancies and early-onset PE pregnancies**

| Characteristic | PC (n=40) | PE (n=45) | *P* value |
|---|---|---|---|
| Maternal age (years) | 28.13±4.28 | 27.49±4.63 | *P*=0.4818 |
| Gestational age (weeks) | 39.57±1.11 | 38.43±2.05 | *P*=0.0022 |
| BMI (kg/m$^2$) | 28.62±0.57 | 30.44±0.63 | *P*=0.0374 |
| Systolic blood pressure (mmHg) | 113.0±1.53 | 145.0±2.18 | *P*<0.0001 |
| Diastolic blood pressure (mmHg) | 73.0±1.20 | 97.0±1.30 | *P*<0.0001 |
| Urine protein/24 h (g) | N/A | 2.86±0.31 | N/A |
| Neonatal birth weight (g) | 3384±65.10 | 3049±106.80 | *P*=0.0111 |
| Fetal gender (male/female) | 17/23 | 26/19 | *P*=0.3316 |

BMI: body mass index

**DNMT1-mediated DNA methylation inhibits TP53BP2 transcription**

First, we analyzed the genomic sequence of the TP53BP2 promoter to evaluate the effect of epigenetic regulation on TP53BP2 expression via the UCSC database. As expected, the TP53BP2 promoter contained a high percentage of GC bases in the CpG islands (**Figure S4A** ). The MethPrimer program identified a single CpG island measuring 1240 base pairs in length. This island spans from position -599 to +641 relative to the transcription start site. It has a CG content of 50% and a CpG ratio of 0.6. This CpG island is located at the distal end of the 5'-flanking region of TP53BP2 (**Figure S4B** ), which may regulate TP53BP2 levels through methylation. Several fragments of the TP53BP2 5'-flanking region were subsequently inserted into the firefly luciferase vector pGL3, and the results of the luciferase activity assay revealed that the -599–35 fragment, which spans most of the CpG dinucleotides of the TP53BP2 promoter, presented the highest promoter activity (**Figure 5A). Consistent with this result** , a luciferase assay revealed increased transcription activity of TP53BP2 in both HTR8/SVneo and JEG-3 cells after the cells were transfected with a luciferase reporter of pGL3 harboring the fragment (-599/-35) (**Figure 5B** ), indicating that this region (-599–35) serves as the core regulatory region for TP53BP2. To examine whether DNA methylation directly represses TP53BP2 promoter activity, we cloned the TP53BP2 proximal promoter region from -599–35. The cloned inserts were then methylated via the methylases Sss I (M.Sss I), Hha I (M.Hha I), and Hpa II (M.Hha II). **Sss I was adopted to methylate all 51 CpG sites within the sequence 5'-CpG-3', Hha I methylated only 9 CpG sites within the sequence 5'-GCGC-3', and Hpa II methylated 3 CpG sites within the sequence 5'-CCGG-3'. Proper methylation of the fragments was confirmed by digestion with the restriction enzymes McrBC (methylation-specific restriction enzyme), Hha I, and Hpa** II (methylation-sensitive restriction enzyme) (**Figure 5C). By transfecting a luciferase reporter vector** into trophoblasts and performing a **luciferase assay, we observed that treatment with three kinds of methylases reduced** TP53BP2 promoter **activity.** Notably, Sss I methylase had the most significant inhibitory effect (**Figure 5D** ). Next, we detected differences in TP53BP2 DNA methylation levels via methylation-specific PCR (MSP). As shown in**Figure 5E, F** , global DNA methylation levels **were decreased** in placentas from **PE pregnancies and trophoblasts** under hypoxia. Bisulfite sequencing PCR (BSP) further revealed a remarkable decrease in DNA methylation levels within the (-599/-35) region of the TP53BP2 promoter in HTR8/SVneo cells under hypoxia (**Figure 5G** ). **These results revealed that DNA hypomethylation modulates the transcriptional activation of TP53BP2 in trophoblasts in the placenta of** PE pregnancies.

To determine the key enzymes involved in DNA methylation, HTR8/SVneo cells were treated with DC_05 (DNMT1 inhibitor), Theaflavin-3, 3'-digallate (TFD, DNMT3a inhibitor) or Nanomycin A (NA, DNMT3b inhibitor) under hypoxia. As shown in **Figure 5H,** DC_05 treatment, but not TFD or NA treatment, caused a significant decrease in the DNA methylation level of the TP53BP2 promoter in HTR8/SVneo cells under hypoxia. To further confirm the role of DNMT1 in regulating TP53BP2 DNA methylation, we constructed HTR8/SVneo cells with DNMT1 knockdown (**Figure S5** ). The results revealed that the knockdown of

DNMT1 decreased the DNA methylation level of the TP53BP2 promoter (**Figure 5I** ) and increased the transcriptional activity and protein levels of TP53BP2 (**Figure 5J, K** ). Taken together, these results suggest that DNMT1-mediated DNA methylation strongly inhibits TP53BP2 expression.

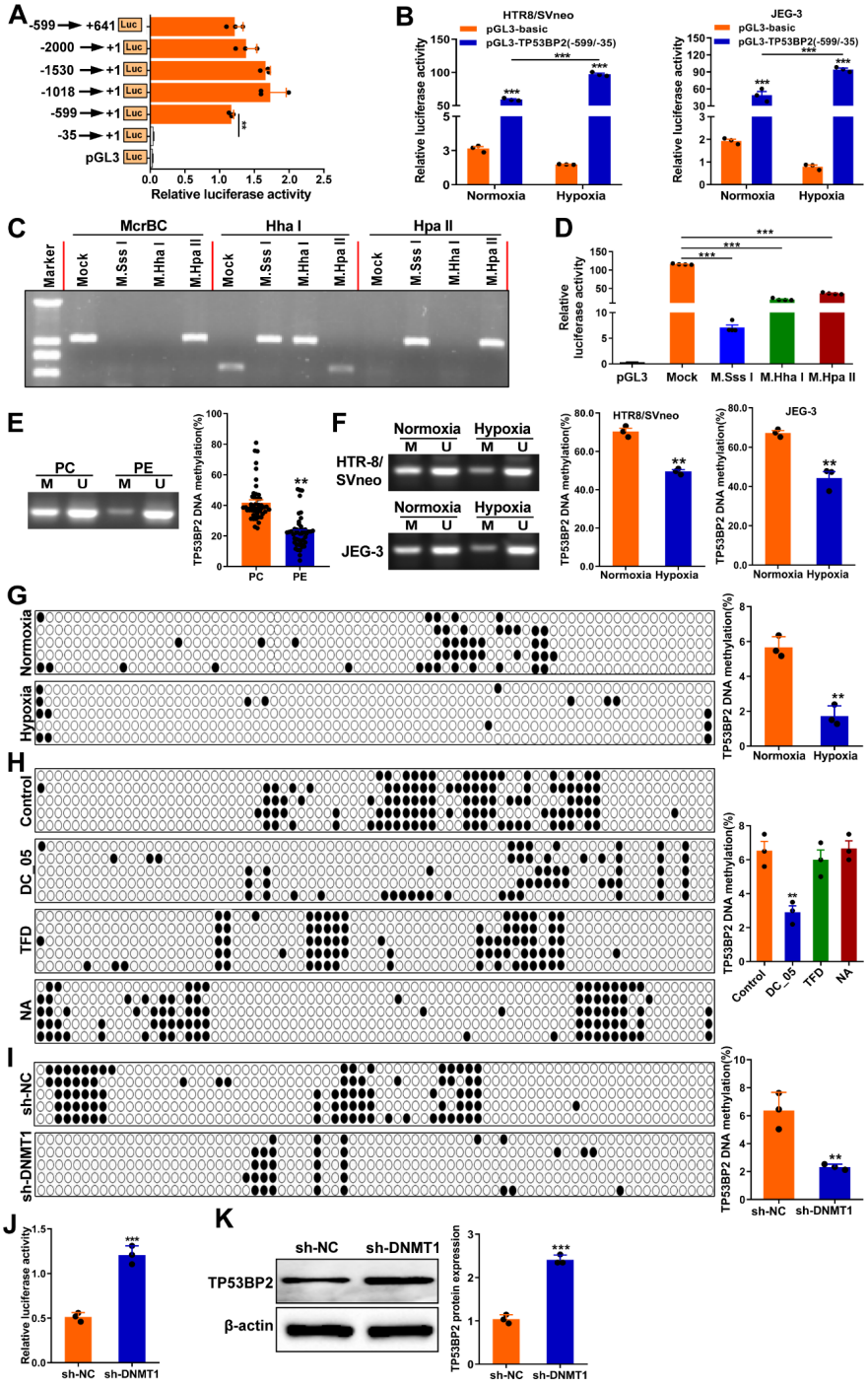


**Figure 5. DNA methylation represses TP53BP2 transcription via DNMT1.** **(A)** The promoter activity of TP53BP2 was evaluated via a dual-luciferase reporter assay. Different fragments of the

TP53BP2 promoter (-35/+1, -599/+1, -1018/+1, -1530/+1, -599/+641, and -2000/+1) were transfected into HEK293T cells with a Renilla luciferase vector (internal control), and the results are presented as firefly luciferase activity normalized to Renilla luciferase activity. **(B)** Dual-luciferase reporter assay analysis of the luciferase activities of the TP53BP2 promoter (-599/-35) in HTR8/SVneo and JEG-3 cells under hypoxia. **(C)** Methylation of the TP53BP2 promoter in HEK293T cells. Following methylation with SssI, HhaI, or HpaII methylases, TP53BP2 promoter fragments were digested with McrBC (a methylation-specific restriction enzyme), HpaII or HhaI (a methylation-sensitive restriction enzyme) to confirm the methylation status of the TP53BP2 promoter construct. **(D)** The activity of the TP53BP2 proximal promoter methylated with SssI, HhaI, or HpaII methylases was assessed via a luciferase reporter assay in HEK293T cells transfected with luciferase reporter constructs. **(E, F)** DNA methylation levels of the TP53BP2 promoter were evaluated via methylation-specific PCR (MSP) in placentas and in HTR8/SVneo and JEG-3 cells under hypoxia. U: unmethylated; M: methylated. **(G)** DNA methylation levels of the TP53BP2 promoter were evaluated via bisulfite sequencing PCR (BSP) in HTR8/SVneo cells under hypoxia. White cycle, unmethylated CpG dinucleotides; black cycle, methylated CpG dinucleotides. The percentage of methylation on each CpG dinucleotide was calculated by the number of methylated clones in each CpG site divided by the total number of clones in the same CpG site and is shown in the right panel. **(H)** The DNA methylation level of the TP53BP2 promoter was evaluated via BSP in HTR8/SVneo cells treated with DC_05 (a DNMT1-specific inhibitor), Theaflavin-3, 3'-digallate (TFD, a DNMT3a-specific inhibitor) or Nanomycin A (NA, a DNMT3b-specific inhibitor) under hypoxia. **(I)** The DNA methylation level of the TP53BP2 promoter was evaluated via BSP in HTR8/SVneo cells transfected with sh-DNMT1 under hypoxia. **(J)** The transcriptional activity of TP53BP2 in HTR8/SVneo cells transfected with sh-DNMT1. **(K)** TP53BP2 expression was evaluated via western blotting in HTR8/SVneo cells transfected with sh-DNMT1 under hypoxia. The data are presented as the means ± SDs. $^{*}P$ <0.05,$^{**}P$ <0.01,$^{***}P$ <0.001.

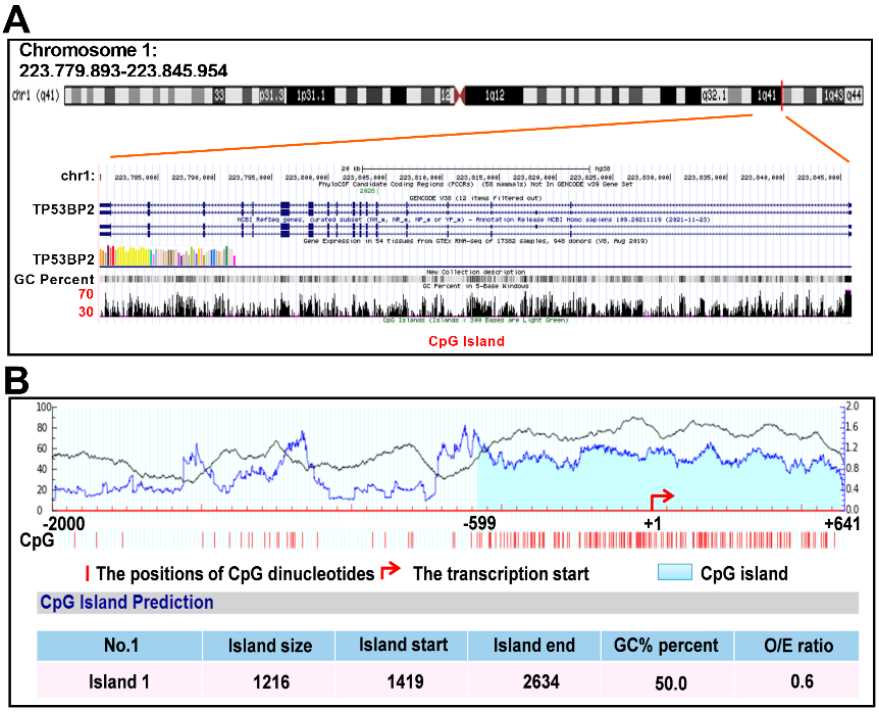


**Figure S4. TP53BP2 transcript analysis. (A)** The UCSC genome browser (http://genome.ucsc.edu) was used to visualize the genomic positioning and organization of TP53BP2, which is located on chromosome 1q41. The genomic region spanning approximately 60 kb is displayed, and gene transcripts are shown in the tracks below the genomic regions. Additionally, the percentages of CpG islands and GCs are shown

in the region below the gene transcript. **(B)** The Meth primer program identified one CpG island of 1240 bp (-599/+641 bp) at the TP53BP2 promoter. The red arrow indicates the transcription start site. The lower limits were as follows: %GC=50, obsCpG/exp CpG=0.60, and length=200 bp. CpG island star=1419, end=2634, %GC=74.4, obsCpG/expCpG=0.944.

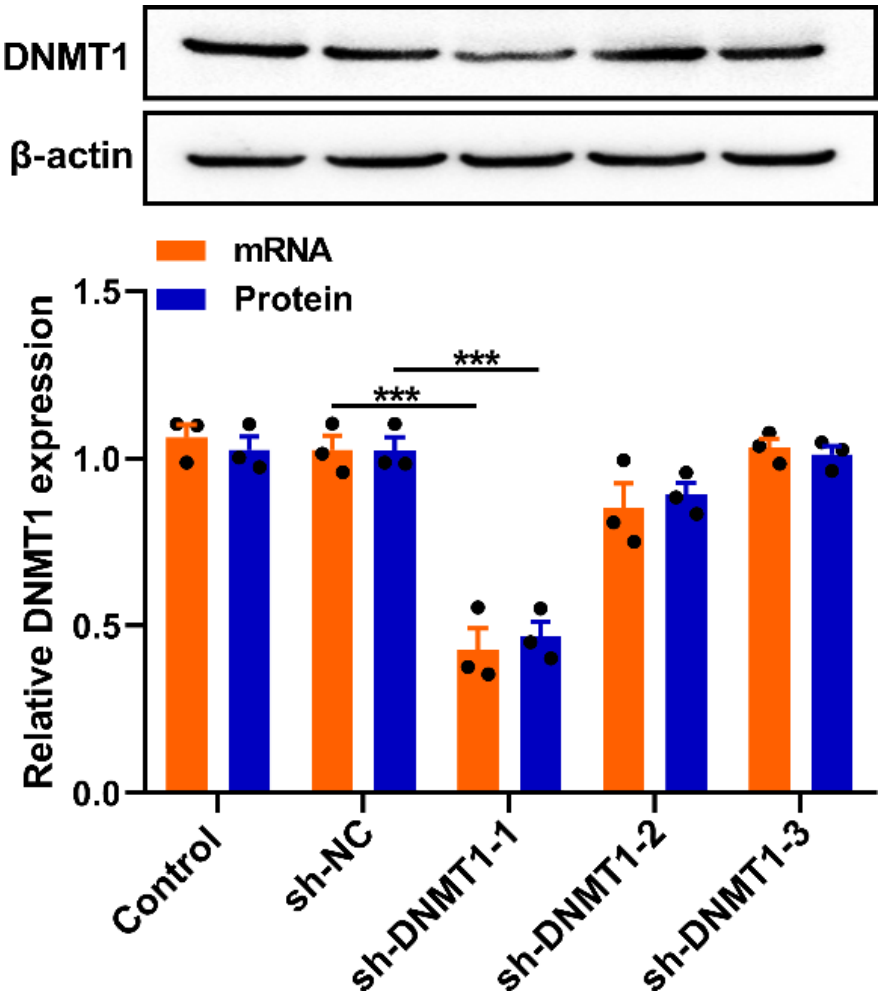


**Figure S5. Expression of DNMT1 in HTR8/SVneo cells.** The expression of DNMT1 was examined by qRT-PCR and western blot in HTR8/SVneo cells transfected with three sh-DNMT1 or sh-NC. Data were presented as the mean ± SD. $^{***}P$ <0.001.

**DNMT1 inhibited TP53BP2 expression via inversely modulating E2F1**

TP53BP2 has been reported to be a direct target of E2F1. Here, both qRT-PCR and western blot **assays revealed** a significant increase in E2F1 **levels in placentas from PE** pregnancies compared with those from non-**PE** pregnancies (**Figure 6A** ). This finding was further confirmed by i**mmunofluorescence staining of trophoblasts from the placentas of PE** pregnancies (**Figure 6B** ). Next, we examined the impact of E2F1 on TP53BP2 expression by overexpressing or knocking down E2F1 in HTR8/SVneo and JEG-3 cells (**Figure S6** ). E2F1 overexpression and E2F1 knockdown increased and inhibited TP53BP2 expression, respectively, in HTR8/SVneo cells under hypoxia (**Figure 6C** ). Furthermore, a chromatin immunoprecipitation (ChIP) assay using an anti-E2F1 antibody revealed significant enrichment of E2F1 at the TP53BP2 promoter under hypoxia (**Figure 6D** ). Next, via the use of the JASPAR database to compute

putative transcription factor binding elements encompassing the hypomethylated CpG site in the TP53BP2 promoter, we identified three putative E2F1 binding sites (**-33/-22, -99/-88 and -368/-357** )**in the TP53BP2 promoter (Figure 6E** ). A ChIP assay revealed remarkable binding of E2F1 with the TP53BP2 promoter at the -33/-22, -99/-88 and -368/-357 sites (**Figure 6F). In addition, a luciferase reporter assay revealed a significant decrease in the activity of the TP53BP2 promoter** after mutation of the -33/-22 site (Mut1), -99/-88 site (Mut2) and -368/-357 site (Mut3) (**Figure 6G** ). As methyltransferases can regulate target gene expression by directly interacting with transcription factors33()**, we th** en adopted the C**o-IP method to investigate the relationship between DNMT1** and E2F1. **Consistent with a previous report, DNMT1 physically interacts with E2F1 in trophoblasts under hypoxia (Figure 6H** ). Moreover, a ChIP assay further revealed that knockdown of DNMT1 increased **the enrichment of E2F1 in the TP53BP2 promoter (Figure 6I). This result demonstrated that** DNMT1 mediated the binding between E2F1 and the TP53BP2 promoter. **Collectively, these data suggest that DNMT1 suppresses E2F1 binding to the** TP53BP2 promoter, resulting in reduced autophagy in trophoblasts under hypoxia.

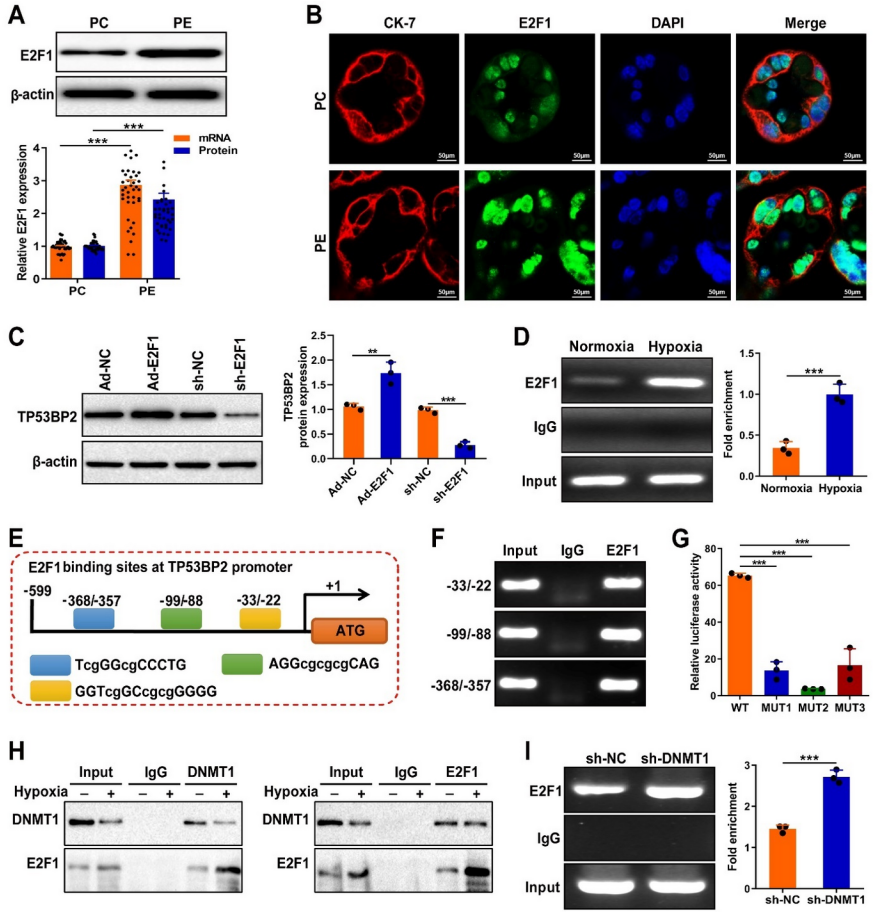


**Figure 6. DNMT1 inhibits TP53BP2 expression by inversely modulating E2F1 in trophoblasts. (A) E2F1 expression in placentas was detected via qRT-PCR and western blotting. (B)** Immunofluorescence staining was used to detect E2F1 expression (green) in trophoblasts of the placenta. Scale bar=50 μm. **(C)** TP53BP2 expression was detected via western blotting in HTR8/SVneo cells transfected with Ad-E2F1 or sh-E2F1 under hypoxia. **(D) The enrichment of E2F1 at the promoter region of TP53BP2 in HTR8/SVneo cells under hypoxia was examined via a ChIP assay with an**

**E2F1 antibody. (E) A schematic diagram of the predicted E2F1-binding sites in the TP53BP2 promoter region from the JASPAR database (http://www.genereg.net/). The blue box represents the -33/-22 site. The green box represents the -99/-88 site. The yellow box represents the -368/-357 site. (F) A ChIP assay was conducted to assess the binding of E2F1 to specific sites (-33/-22, -99/-88, and -368/-357) on the TP53BP2 promoter in HTR8/SVneo cells under hypoxia. (G)** The promoter activities of TP53BP2 with the wild-type (WT) or mutant -33/-22 site (Mut1), -99/-88 site (Mut2) and -368/-357 site (Mut3) of E2F1 were determined via a luciferase reporter assay in HEK293T cells. **(H)** Co-IP assay followed by immunoblotting showing the interactions between DNMT1 and E2F1 in HTR8/SVneo cells under hypoxia. **(I)** A ChIP assay was performed to demonstrate that E2F1 binds to the TP53BP2 promoter in HTR8/SVneo cells transfected with sh-DNMT1. The data are presented as the means ± SDs. $^{**}P$ <0.01,$^{***}P$ <0.001.

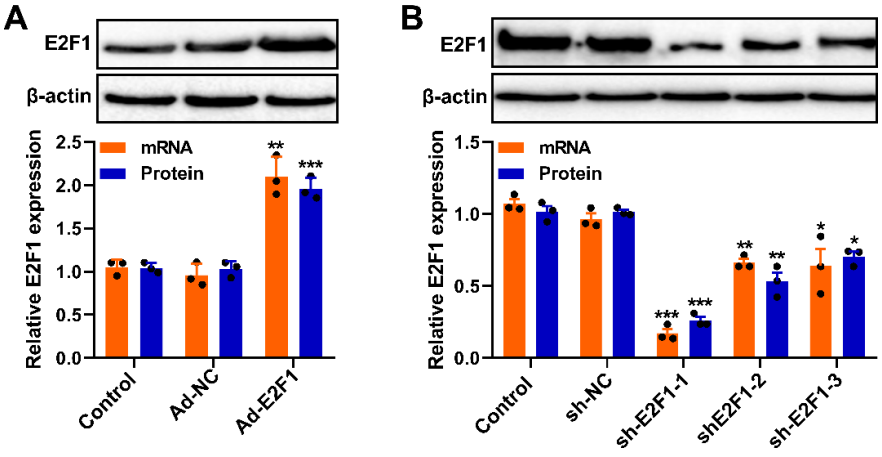


**Figure S6. Expression of E2F1 in HTR8/SVneo cells. (A, B)** The expression of ASPP2 in HTR8/SVneo cells transfected with Ad-E2F1 or sh-E2F1 was examined via qRT-PCR and western blotting. The data are presented as the means ± SDs. $^{*}P$ <0.05,$^{**}P$ <0.01,$^{***}P$ <0.001.

### G9a-mediated histone methylation inhibits TP53BP2 transcription in trophoblasts

Histone modifications play important roles in the regulation of gene transcription34(). We used ENCODE Histone Modification Tracks embedded in the UCSC Genome Browser and identified 7 histone modifications (H3K4me1, H3K4me2, H3K4me3, H3K9me2, H3K9me3, H3K27me3 and H3K36me3) in the TP53BP2 promoter region. Among these histone modifications, H3K4me2 and H3K4me3 presented the greatest number of enrichment peaks (**Figure 7A** ). By performing a ChIP assay, we only detected a significant reduction in H3K9me2 enrichment at the TP53BP2 promoter in HTR8/SVneo cells under hypoxia, but not in other cells (**Figure 7B** ). Immunofluorescence staining revealed a significant decrease in **H3K9me2 levels in placental trophoblasts from PE** pregnancies (**Figure 7C** ). This result also suggested the importance of H3K9me2 in TP53BP2 transcription **in the trophoblasts of PE** pregnancies. Furthermore, by measuring the levels of several widely recognized histone methyltransferases (HMTs), including G9a, LSD1, SUV39H1 and SUV39H2, we detected significant decreases in G9a levels **in placentas from PE** pregnancies and in HTR8/SVneo cells under hypoxia (**Figure 7D, E** ). In vitro assays demonstrated that G9a knockdown in HTR8/SVneo cells (**Figure S7** ) significantly upregulated TP53BP2 transcription under hypoxia (**Figure 7F** ). Similarly, treatment with BIX-01294 (a G9a-specific inhibitor) also increased the level of TP53BP2 in HTR8/SVneo cells under hypoxia (**Figure 7G** ). These data demonstrated that G9a can inhibit TP53BP2 expression in the placentas of PE pregnancies.

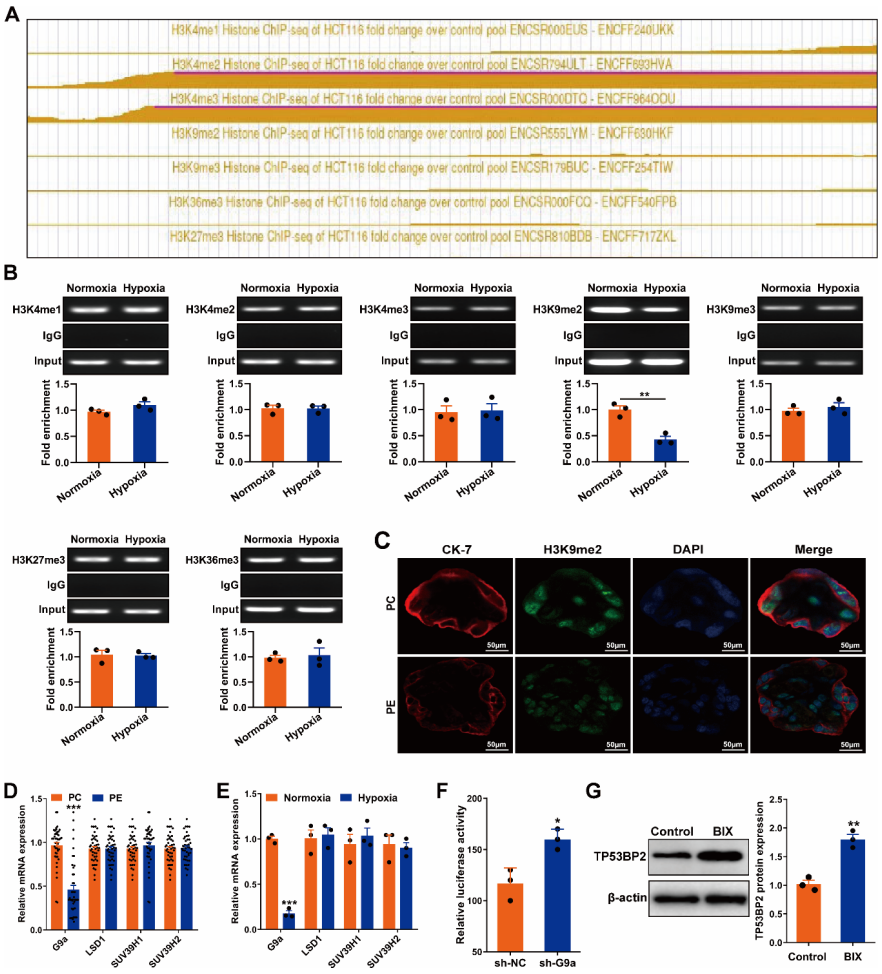


**Figure 7. TP53BP2 is inhibited by G9a-mediated histone methylation in trophoblasts.** **(A)** H3K4me1, H3K4me2, H3K4me3, H3K9me2, H3K9me3, H3K27me3 and H3K36me3 modifications were detected in the TP53BP2 promoter region. **(B)** ChIP assays were conducted to assess the enrichment of H3K4me1, H3K4me2, H3K4me3, H3K9me2, H3K9me3, H3K27me3 and H3K36me3 at the TP53BP2 promoter in HTR8/SVneo cells under hypoxia. **(C)** Immunofluorescence staining was used to detect the expression of H3K9me2 (green) in trophoblasts of the placenta. Scale bar=50 μm. **(D, E)** The mRNA expression levels of LSD1, SUV39H1, SUV39H2 and G9a were measured via qRT-PCR in placentas and in HTR8/SVneo cells under hypoxia. **(F)** The transcriptional activity of the TP53BP2 promoter in HTR8/SVneo cells transfected with sh-G9a under hypoxia. **(G)** The expression of TP53BP2 in HTR8/SVneo cells treated with BIX-01294 (a G9a-specific inhibitor) under hypoxia was detected via western blotting. The data are presented as the means ± SDs. $^{*}P$ <0.05,$^{**}P$ <0.01,$^{***}P$ <0.001.

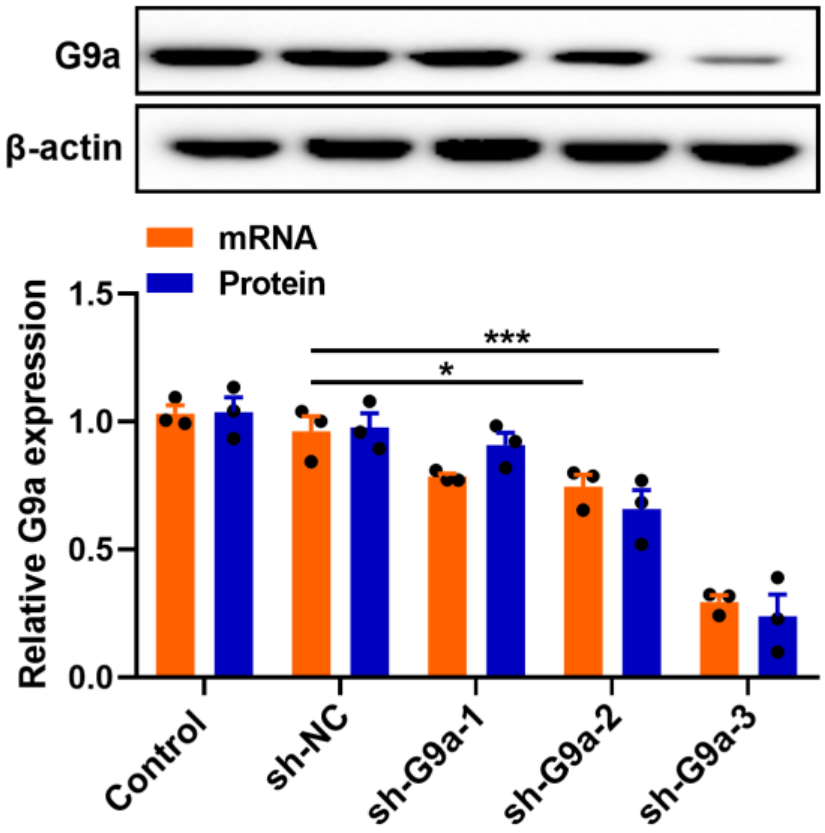


**Figure S7. Expression of G9a in HTR8/Svneo cells.** The expression of G9a in HTR8/SVneo cells transfected with sh-G9a or sh-NC was examined via qRT-PCR and western blotting. The data are presented as the means ± SDs. $^{*}P$ <0.05,$^{***}P$ <0.001.

**G9a and DNMT1 cooperatively suppress the binding of E2F1 to TP53BP2**

To elucidate the potential relationship between DNMT1 and G9a in regulating TP53BP2 expression, DNMT1 or G9a was overexpressed in HTR8/SVneo cells via Ad-DNMT1 and/or Ad-G9a transfection (**Figure S8). Overexpression of DNMT1 or G9a decreased E2F1 binding to the TP53BP2 promoter, whereas co-overexpression of both DNMT1 and G9a further attenuated this binding (Figure 8A). Moreover,** knockdown of both G9a and DNMT1 significantly decreased TP53BP2 DNA methylation levels and H3K9me2 enrichment at the TP53BP2 promoter in HTR8/SVneo cells under hypoxia (**Figure 8B, C** ), ultimately resulting in significant upregulation of TP53BP2 transcription and protein expression (**Figure 8D, E** ). Similar results were also observed in HTR8/SVneo cells treated with DC_05 or/and BIX under hypoxia (**Figure S9** ). Notably, the injection of AAV-shG9a or/and AAV-shDNMT1 into the placenta of PE rats significantly increased placental damage, as evidenced by HE staining (**Figure 8F** ). Additionally, PE rats injected with AAV-shG9a or/and AAV-shDNMT1 presented significant increases in blood pressure and urinary protein levels **(Figure 8G, H** ), suggesting a synergistic inhibitory effect of G9a and DNMT1 on E2F1 binding to the TP53BP2 promoter in placental dysfunction. Next, we investigated the interactions among E2F1, DNMT1 and G9a in trophoblasts. Co-IP assays revealed that DNMT1 physically interacted with G9a and E2F1 in HTR8/SVneo cells under hypoxia, whereas there was almost no interaction between G9a and**E2F1 (Figure 8I** ). Immunofluorescence staining revealed that both DNMT1 and G9a were colocalized with E2F1 **in the nuclei of HTR8/SVneo cells (Figure 8J).** Considering the multiple functional domains of DNMT1, we constructed a series of truncated constructs of DNMT1, and plasmids

encoding different GST-tagged DNMT1 fragments (GST-Control, GST-WT, GST-1-446, GST-431-703, GST-643-835, GST-836-1060, and GST-1061-1632) were cotransfected **with plasmids encoding Myc-tagged G9a (Myc-G9a) or Flag-tagged E2F1 (Flag-E2F1) into HEK293 cells (Figure 8K** ). Co-IP assays revealed that the 1–446 region of DNMT1 interacted with G9a, whereas the 1061–1632 region of DNMT1 interacted **with E2F1 (Figure 8L** ). Most importantly, a qRT-PCR assay revealed a marked increase in TP53BP2 expression in HTR8/SVneo cells transfected with the Δ1-446 mutation, whereas transfection with the Δ1061-1632 mutation de**creased its expression (Figure 8M** ). Furthermore, we constructed plasmids with a deleted region of DNMT1 that interacts with G9a (Δ1-446) or E2F1 (Δ1061-1632) and transfected these mutants into HTR8/SVneo cells. Interestingly, deletion of the 1-446 region of DNMT1 markedly increased the enrichment of E2F1 at the TP53BP2 promoter in HTR8/SVneo cells under hypoxia while reducing the enrichment of DNMT1 at the TP53BP2 promoter. On the other hand, deletion of the 1061–1632 region of DNMT1 promoted E2F1 **binding at the TP53BP2 promoter and enhanced H3K9me2 enrichment (Figure 8N). Collectively, these data indicate that the interaction between G9a and DNMT1 can suppress E2F1-mediated activation of TP53BP2 in trophoblasts** .

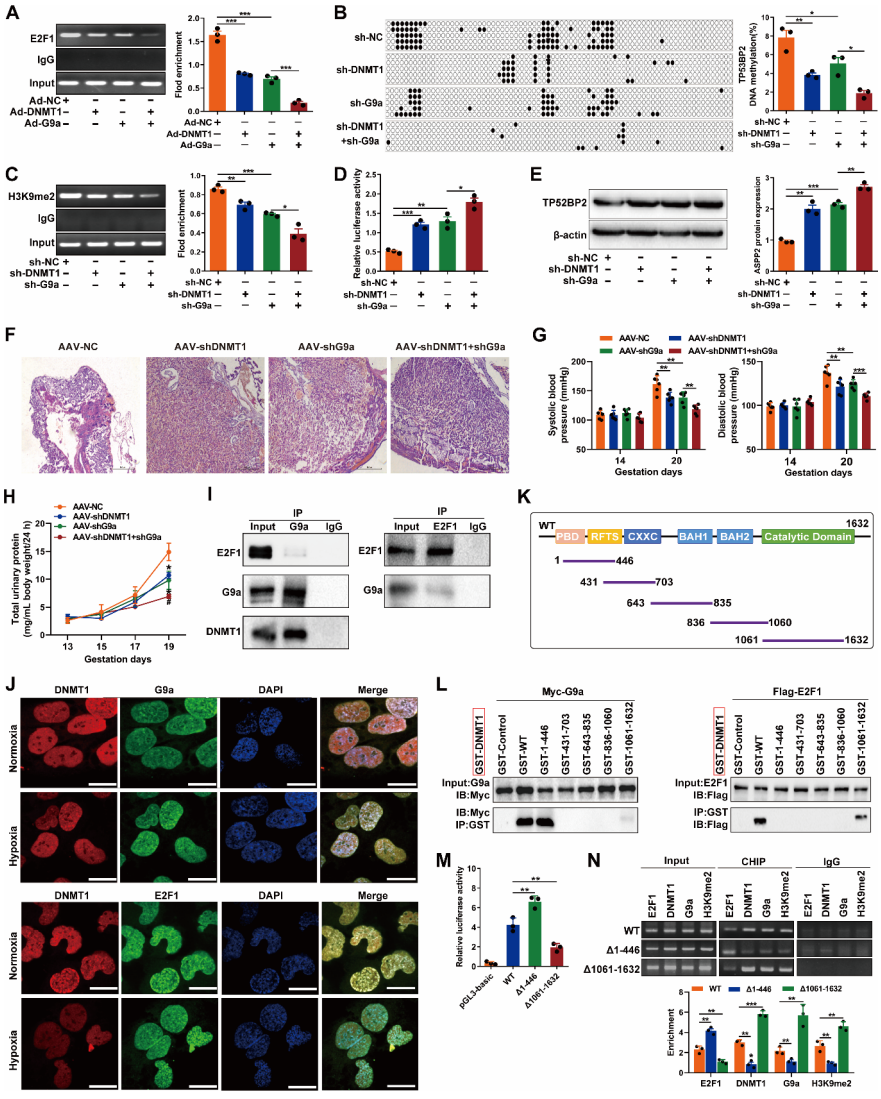


**Figure 8. DNMT1 and G9a cooperatively regulate TP53BP2 expression in PE. (A)** Enrichment

of E2F1 at the promoter region of TP53BP2 was analyzed via ChIP in HTR8/SVneo cells transfected with Ad-DNMT1 and/or Ad-G9a under hypoxia. **(B)** BSP analysis was performed to determine the TP53BP2 DNA methylation level in HTR8/SVneo cells transfected with sh-DNMT1 and/or sh-G9a under hypoxia.**(C)** H3K9me2 enrichment at the promoter region of TP53BP2 was analyzed via ChIP in HTR8/SVneo cells transfected with sh-DNMT1 and/or sh-G9a under hypoxia. **(D)** The promoter transcription activity of TP53BP2 was analyzed via a dual-luciferase reporter assay in HTR8/SVneo cells transfected with sh-DNMT1 and/or sh-G9a under hypoxia.**(E)** Western blotting was performed to determine TP53BP2 expression in HTR8/SVneo cells transfected with sh-DNMT1 and/or sh-G9a under hypoxia. **(F)** Placental pathological changes in PE rats injected with AAV-shG9a and/or AAV-shDNMT1 were evaluated via HE staining. Scale bars=500 μm. **(G)** Noninvasive tail-cuff blood pressure measurement system used to detect the systolic blood pressure and diastolic blood pressure of PE rats injected with AAV-shG9a and/or AAV-shDNMT1. **(H)** Total urine protein levels in PE rats injected with AAV-shG9a and/or AAV-shDNMT1. **(I)** Co-IP assay followed by immunoblotting showing the interactions between G9a and DNMT1 or E2F1 in HTR8/SVneo cells under hypoxia. **(J)** Immunofluorescence staining was used to measure the colocalization of DNMT1 (red) and E2F1 (green) or G9a (green) in HTR8/SVneo cells under hypoxia. Nuclei were stained with DAPI. Scale bar=20 μm. **(K)** Schematic diagram depicting the structure of DNMT1 and truncation mutants of the GST-tagged DNMT1 fragments (GST-Control, GST-WT, GST-1-446, GST-431-703, GST-643-835, GST-836-1060, and GST-1061-1632). **(L)** The interactions between DNMT1 and G9a or between DNMT1 and E2F1 were examined via Co-IP with an anti-Myc antibody in HEK293T cells cotransfected with plasmids encoding different GST-tagged DNMT1 fragments and plasmids encoding Myc-tagged G9a (Myc-G9a) or Flag-tagged E2F1 (Flag-E2F1), respectively.**(M)** The transcriptional activity of the TP53BP2 promoter in HTR8/SVneo cells transfected with the Δ1-446 mutation or the Δ1061-1632 mutation. **(N)** The enrichment of E2F1, DNMT1, G9a and H3K9me2 at the promoter region of TP53BP2 in HTR8/SVneo cells transfected with wild-type DNMT1 (WT), the G9a binding region deletion mutant DNMT1 (Δ1-446) or the E2F1 binding region deletion mutant DNMT1 (Δ1061-1632) was assessed via a ChIP assay under hypoxia. The data are presented as the means±SDs. Student's t test (unpaired, two-tailed) was used to compare two independent groups, and two-way ANOVA was performed for comparisons of multiple groups.$^{*}P$ <0.05,$^{**}P$ <0.01,$^{***}P$ <0.001;$^{\#}P$ <0.05.

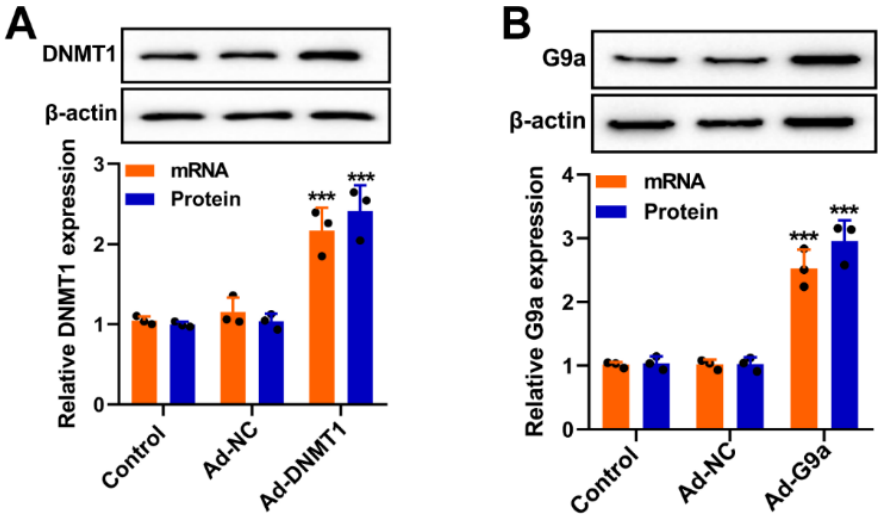


**Figure S8. Expression of DNMT1 and G9a in HTR8/Svneo cells. (A, B)** The expression of DNMT1 and G9a was examined by qRT-PCR and western blot in HTR8/SVneo cells transfected with Ad-DNMT1 or Ad-G9a. Data were presented as the mean ± SD. Student's t test (unpaired, two-tailed) was used to compare two independent groups.$^{***}P$ <0.001.

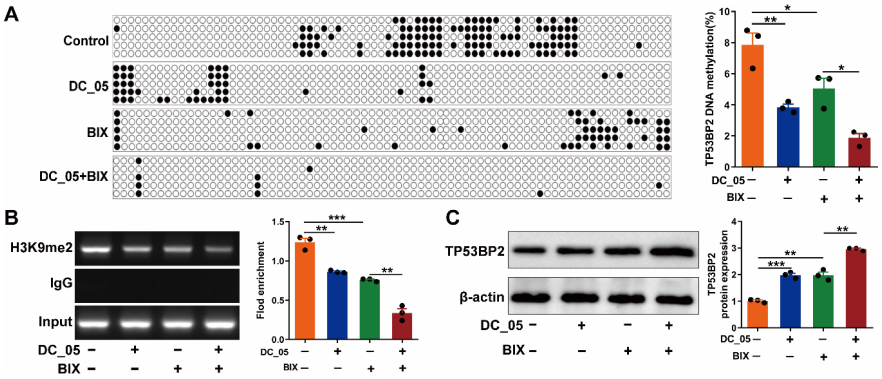


**Figure S9. Effects of DC_05 and BIX on TP53BP2 DNA methylation, H3K9me2 and H3K9me2 expression in HTR8/Svneo cells.** **(A)** BSP analysis was performed to determine the TP53BP2 DNA methylation level in HTR8/SVneo cells under hypoxia. **(B)** H3K9me2 enrichment at the TP53BP2 promoter in HTR8/SVneo cells under hypoxia was assessed via a ChIP assay. **(C)** TP53BP2 expression in HTR8/SVneo cells under hypoxia was determined by western blotting. The data are presented as the means ± SDs. $^{*}P$ <0.05,$^{**}P$ <0.01,$^{***}P$ <0.001.

## Discussion

**PE is a condition that typically occurs after the 20th week of pregnancy and is characterized by high blood pressure and often the presence of protein in the urine (proteinuria)35()** . Moreover, clinical evidence indicates that leaving the placenta from the mother can alleviate symptoms in patients with PE36(). As a conserved process in eukaryotes that maintains cellular homeostasis5(), autophagy can be activated in PE cases and trophoblasts under hypoxia37(). Thus, it has been identified as a target for therapeutic intervention in **PE, which supports** our findings that excessive autophagy occurs in placentas from PE pregnancies and in trophoblasts under hypoxia. However, the specific mechanism of placental dysfunction caused by excessive autophagy should be further explored. Here, we demonstrated that TP53BP2 could induce trophoblast autophagy in placentas from early-onset **PE pregnancies. Mechanistically, we found that DNMT1-mediated DNA hypomethylation and G9a-mediated H3K9me2 suppressed** the binding of E2F1 to the TP53BP2 promoter, eventually inhibiting **TP53BP2 expression and autophagy in trophoblasts during PE pregnancies. Moreover, TP53BP2 was found to be a predictive biomarker associated with the clinicopathological characteristics of** early-onset **PE** and a promising target for the treatment of early-onset PE.

As a p53-binding protein, TP53BP2 can promote p53-mediated apoptosis12(). Recent studies have shown that TP53BP2 is involved in the regulation of diverse diseases through interactions with different molecules. For example, TP53BP2 was found to mitigate acute kidney injury induced by ischemia-reperfusion by promoting LC3B-II conversion and facilitating p62 degradation 38(). Similarly, Wang *et al* discovered that TP53BP2 could attenuate HBV replication in hepatocytes through binding to HSF1, thereby inhibiting the transactivation of Atg7 in a p53-independent manner39(). TP53BP2 can also inhibit RAS-induced senescence by preventing the formation of the ATG16-ATG5-ATG12 complex40(). In this study, we not only detected high expression of **TP53BP2 in placentas** from **PE** pregnancies and trophoblasts under hypoxia but also demonstrated that TP53BP2 knockdown alleviated **the pathological process of PE via the inhibition of autophagy in trophoblasts. Moreover** , TP53BP2 induced autophagy by promoting the release of Beclin-1 from the Beclin-1-Bcl-2 complex in trophoblasts. However, more investigations are needed to elucidate the detailed mechanism involved.

Epigenetic regulation of gene expression involves several mechanisms, including DNA methylation, histone modification, and the biogenesis and action of noncoding RNAs40(). They regulate gene expression by modulating the accessibility of transcription factors and other regulatory proteins to DNA. Pregnancy involves

dynamic genetic and epigenetic modifications that are essential for the development and health of both the mother and the fetus. These modifications encompass a range of processes that influence gene expression, chromatin structure, and cellular function throughout gestation 41(). DNA methylation is a fundamental epigenetic mechanism that usually occurs at cytosine-guanine dinucleotide (CpG) sites and is typically mediated by DNMTs (DNMT1, DNMT3a and DNMT3b)42(). Studies have reported that DNA methylation regulates diverse biological processes, including chromatin structure remodeling, gene transcription, genome imprinting, and chromosome stability43-45(). In addition, the processes of pregnancy, including fertilization, embryo implantation, and placental development during early human early embryo development, are intricately intertwined with DNA methylation45(). Therefore, it is reasonable to hypothesize that PE could be linked to abnormal DNA methylation patterns in crucial genes. As expected, the TP53BP2 promoter contains a high percentage of GC bases in the form of CpG islands, and the TP53BP2 DNA methylation level is markedly decreased in PE. Moreover, the present study revealed that the suppression of DNMT1 binding between**E2F1 and the TP53BP2 promoter** contributes to the inhibition of TP53BP2 transcription in trophoblasts. In turn, the inhibition of DNMT1 expression significantly increases TP53BP2 expression by decreasing its methylation, suggesting that the upregulation of TP53BP2 is mediated in a DNA methylation-dependent manner.

More importantly, as a transcription activator, after dimerization with partner proteins, E2F1 binds to DNA via the E2 recognition site of 5'-TTTC[CG]CGC-3' in the promoter region of various genes46(). E2F1 is overexpressed in cancers such as lung cancer, colorectal cancer, and bladder cancer, as well as sporadic Burkitt's lymphomas4748(,). Consistent with these reports**, E2F1 is highly expressed in placentas** from **PE** pregnancies and trophoblasts under hypoxia. A previous study reported that E2F1 regulates cell growth and increases cell size through the activation of mTORC1, a major regulator of protein synthesis and autophagy49(). In addition, in the context of obesity, high levels of E2F1 in adipose tissue can induce the expression of autophagy-related genes and activate autophagy50(). Consistent with this observation, our results indicated that high levels of E2F1 significantly upregulated TP53BP2 expression and autophagy in trophoblasts under hypoxia. Moreover, our work identified three putative E2F1 binding sites in the TP53BP2 promoter.

In addition, by observing **the role of histone methylation in the pathogenesis of PE** , we demonstrated that, under hypoxia, the enrichment of H3K9me2 at the TP53BP2 promoter was noticeably reduced in HTR8/SVneo cells, accompanied by the activation of TP53BP2. Our results further indicated that the reduction in H3K9me2 enrichment was attributed to the downregulation of G9a and reduced recruitment of G9a to the TP53BP2 promoter in HTR8/SVneo cells under hypoxia. Notably, DNA methylation and histone modification can often cooperatively regulate gene expression by modifying chromatin structure51(). In this study, we found that cooperative inhibition of DNMT1 and G9a led to TP53BP2 activation, transcription and trophoblast autophagy in PE. Multiple mechanisms can explain the change in TP53BP2 transcription. First, DNA methylation and histone modification share the same methyl donor. Second, the physical interaction between DNMT1 and G9a suggests a potential mechanism for coordinating DNA methylation and histone modification of chromatin regions in vivo during replication52(). Moreover, H3K9me2 can act as a docking site for chromatin-modifying proteins and heterochromatin proteins. This interaction subsequently recruits DNMT1 and enhances its activity, resulting in DNA hypermethylation53(). In addition, decreased DNMT1 and G9a promote E2F1 binding to the TP53BP2 promoter, leading to the upregulation of TP53BP2 in trophoblasts. This may occur through the inhibition of the formation of compact and active chromatin structures, thereby making the region accessible to E2F1. This observation was supported by our previous finding that DNA methylation and H3K9ac are involved in the reduction of miR-195-3p in Hcy-induced atherosclerosis54(). Intriguingly, G9a restrains the enrichment of E2F1 in the TP53BP2 promoter via direct interaction with amino acids 1–446 of DNMT1 but not E2F1.

In conclusion, the interplay between H3K9me2 and DNA hypomethylation cooperatively suppresses TP53BP2 transcription by inhibiting the binding of E2F1 to the TP53BP2 promoter, leading to excessive trophoblast autophagy and consequently the development of PE. Therefore, TP53BP2 may be a new independent biomarker for the diagnosis or prognostic prediction of early-onset PE (**Fig 9** ).

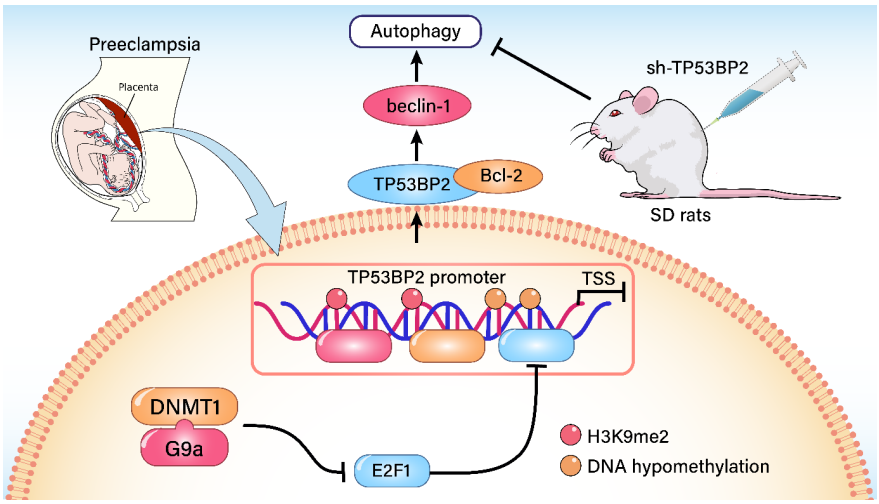


**Fig. 9 TP53BP2 promotes placental autophagy and preeclampsia via G9a, and DNMT1 cooperatively modulates E2F1. The inhibition of TP53BP2 expression attenuated the progression of PE by inhibiting the autophagy of trophoblasts in SD rats, which was attributed to the fact that G9a-mediated H3K9me2- and DNMT1-mediated DNA hypomethylation suppressed the binding of E2F1 at the TP53BP2 promoter to suppress the expression of TP53BP2 transcription and subsequently inhibited the release of Beclin-1 from the Bcl-2-Beclin-1 complex.**

## Acknowledgments

This work was supported by the grants from the National Natural Science Foundation of China (82370293, 82270492,82171682, 81900273 ,82371598); Key Research and Development Projects in Ningxia Province (2023BEG02074, 2022BFH02013, 2022BEG02054, 2021BEG02028); Major Scientific Research Project for High level Health Talents in Hunan Province (R2023120). The Open competition mechanism to select the best candidates for key research projects of Ningxia medical university (Nos.XJKF240301 and XJKF240304); The Natural Science Foundation of Ningxia Hui Autonomous Region (Nos. 2023AAC005035).

## Competing interests

The authors declare that no competing interests exist.

## Date availability

**The authors confirm that the data supporting the findings of this study are available within the article and its supplementary materials.**

## References

1. Emeruwa, U.N., Gyamfi-Bannerman, C. and Laurent, L.C. (2023) Biomarkers and the Risk of Preeclampsia. *Jama* , **329** , 539-541.2. Soobryan, N., Reddy, K., Ibrahim, U.H., Moodley, J., Kumar, A. and Mackraj, I. (2024) Identification of gene signature markers in gestational hypertension and early-onset preeclampsia. *Placenta* ,**145** , 1-8.3. Huang, C., Wei, K., Lee, P.M.Y., Qin, G., Yu, Y. and Li, J. (2022) Maternal hypertensive disorder of pregnancy and mortality in offspring from birth to young adulthood: national population based cohort study. *BMJ* , **379** , e072157.4. Sacks, D.A. and Incerpi, M.H. (2024) Of Aspirin, Preeclampsia, and Racism. *N Engl J Med* , **390** , 968-969.5. Vargas, J.N.S., Hamasaki, M., Kawabata, T., Youle, R.J. and Yoshimori, T. (2023) The mechanisms and roles of selective autophagy in mammals. *Nat Rev Mol Cell Biol* , **24** , 167-185.6. Li, C., Liu, W., Lao, Q., Lu, H. and Zhao, Y. (2022) Placenta autophagy is closely associated with preeclampsia. *Aging* , **14** .7. Ling, Q., Zhang, Y.-F., Chang, W., Liu, S.-T., Zhu, H.-L. and Wang, H. (2024) NBR1-dependent autophagy activation protects against environmental cadmium-evoked placental

trophoblast senescence. *Chemosphere* , **358** , 142138.8. Chen, Y., Xiao, L., Xu, J., Wang, J., Yu, Z., Zhao, K., Zhang, H., Cheng, S., Sharma, S., Liao, A. *et al.* (2023) Recent insight into autophagy and immunity at the maternal-fetal interface. *J Reprod Immunol* , **155** , 103781.9. Ma, F., Ding, N., Xie, L., Zhao, X., Ma, S., Li, G., Hao, Y., Xiong, J., Wu, K., Jiang, Y. *et al.* (2024) Inhibition of autophagy via 3-methyladenine alleviates the progression of preeclampsia. *Acta Biochim Biophys Sin (Shanghai)* .10. Guan, G., Zhang, T., Ning, J., Tao, C., Gao, N., Zeng, Z., Guo, H., Chen, C.-C., Yang, J., Zhang, J. *et al.* (2024) Higher TP53BP2 expression is associated with HBsAg loss in peginterferon-α-treated patients with chronic hepatitis B. *J Hepatol* , **80** , 41-52.11. Micheal, S., Saksens, N.T.M., Hogewind, B.F., Khan, M.I., Hoyng, C.B. and den Hollander, A.I. (2018) Identification of TP53BP2 as a Novel Candidate Gene for Primary Open Angle Glaucoma by Whole Exome Sequencing in a Large Multiplex Family.*Mol Neurobiol* , **55** , 1387-1395.12. Huo, Y., Cao, K., Kou, B., Chai, M., Dou, S., Chen, D., Shi, Y. and Liu, X. (2023) TP53BP2: Roles in suppressing tumorigenesis and therapeutic opportunities.*Genes Dis* , **10** , 1982-1993.13. Braithwaite, A.W., Del Sal, G. and Lu, X. (2006) Some p53-binding proteins that can function as arbiters of life and death. *Cell death and differentiation* ,**13** , 984-993.14. Wu, T., Song, H., Xie, D., Zhao, B., Xu, H., Wu, C., Hua, K., Deng, Y., Ji, C., Hu, J. *et al.* (2018) Silencing of ASPP2 promotes the proliferation, migration and invasion of triple-negative breast cancer cells via the PI3K/AKT pathway. *Int J Oncol* , **52** , 2001-2010.15. Wang, Y., Wang, X.D., Lapi, E., Sullivan, A., Jia, W., He, Y.W., Ratnayaka, I., Zhong, S., Goldin, R.D., Goemans, C.G. *et al.* (2012) Autophagic activity dictates the cellular response to oncogenic RAS. *Proc Natl Acad Sci U S A* ,**109** , 13325-13330.16. Liu, Z., Qiao, L., Zhang, Y., Zang, Y., Shi, Y., Liu, K., Zhang, X., Lu, X., Yuan, L., Su, B. *et al.* (2017) ASPP2 Plays a Dual Role in gp120-Induced Autophagy and Apoptosis of Neuroblastoma Cells. *Front Neurosci* , **11** , 150.17. Yao, J., Yang, H., Wang, H., Shi, H., Jiao, Y., Zhang, Y., Chen, D. and Shi, H. (2022) ASPP2 Coordinates ERS-Mediated Autophagy and Apoptosis Through mTORC1 Pathway in Hepatocyte Injury Induced by TNF-α. *Front Pharmacol* , **13** , 865389.18. Sa, R., Ma, J., Yang, J., Li, D.F., Du, J., Jia, J.C., Li, Z.Y., Huang, N., A, L., Sha, R. *et al.* (2023) High TXNIP expression accelerates the migration and invasion of the GDM placenta trophoblast. *BMC Pregnancy Childbirth* ,**23** , 235.19. Li, S., Li, L., Zhang, C., Fu, H., Yu, S., Zhou, M., Guo, J., Fang, Z., Li, A., Zhao, M. *et al.* (2023) PM2.5 leads to adverse pregnancy outcomes by inducing trophoblast oxidative stress and mitochondrial apoptosis via KLF9/CYP1A1 transcriptional axis.*Elife* , **12** .20. Knihtilä, H.M., Kachroo, P., Shadid, I., Raissadati, A., Peng, C., McElrath, T.F., Litonjua, A.A., Demeo, D.L., Loscalzo, J., Weiss, S.T. *et al.* (2023) Cord blood DNA methylation signatures associated with preeclampsia are enriched for cardiovascular pathways: insights from the VDAART trial.*EBioMedicine* , **98** , 104890.21. Garau, J., Charras, A., Varesio, C., Orcesi, S., Dragoni, F., Galli, J., Fazzi, E., Gagliardi, S., Pansarasa, O., Cereda, C. *et al.* (2023) Altered DNA methylation and gene expression predict disease severity in patients with Aicardi-Goutières syndrome. *Clinical immunology (Orlando, Fla.)* , **249** , 109299.22. Preissl, S., Gaulton, K.J. and Ren, B. (2023) Characterizing cis-regulatory elements using single-cell epigenomics. *Nat Rev Genet* , **24** , 21-43.23. Nabais, M.F., Gadd, D.A., Hannon, E., Mill, J., McRae, A.F. and Wray, N.R. (2023) An overview of DNA methylation-derived trait score methods and applications. *Genome biology* , **24** , 28.24. Kim, J., Lee, H., Yi, S.-J. and Kim, K. (2022) Gene regulation by histone-modifying enzymes under hypoxic conditions: a focus on histone methylation and acetylation. *Exp Mol Med* , **54** , 878-889.25. Papanicolau-Sengos, A. and Aldape, K. (2022) DNA Methylation Profiling: An Emerging Paradigm for Cancer Diagnosis. *Annual review of pathology* , **17** , 295-321.26. Barcena-Varela, M., Paish, H., Alvarez, L., Uriarte, I., Latasa, M.U., Santamaria, E., Recalde, M., Garate, M., Claveria, A., Colyn, L. *et al.* (2021) Epigenetic mechanisms and metabolic reprogramming in fibrogenesis: dual targeting of G9a and DNMT1 for the inhibition of liver fibrosis. *Gut* ,**70** , 388-400.27. Sun, S., Aguirre-Gamboa, R. and Barreiro, L.B. (2023) Transmission of stimulus-induced epigenetic changes through cell division is coupled to continuous transcription factor activity.*Frontiers in immunology* , **14** , 1129577.28. Kassab, A., Gupta, I. and Moustafa, A.-E.A. (2023) Role of E2F transcription factor in oral cancer: Recent insight and advancements. *Seminars in cancer biology* , **92** , 28-41.29. Manickavinayaham, S., Velez-Cruz, R., Biswas, A.K., Chen, J., Guo, R. and Johnson, D.G. (2020) The E2F1 transcription factor and RB tumor suppressor moonlight as DNA repair factors. *Cell Cycle* , **19** , 2260-2269.30. Al-Kharashi, L.A., Bakheet, T., AlHarbi, W.A., Al-Moghrabi, N. and Aboussekhra, A. (2021) Eugenol modulates genomic methylation and inactivates breast cancer-associated fibroblasts through E2F1-dependent downregulation of

DNMT1/DNMT3A. *Molecular carcinogenesis* ,**60** , 784-795.31. Ashok, C., Ahuja, N., Natua, S., Mishra, J., Samaiya, A. and Shukla, S. (2021) E2F1 and epigenetic modifiers orchestrate breast cancer progression by regulating oxygen-dependent ESRP1 expression. *Oncogenesis* , **10** , 58.32. Xie, L., Ding, N., Sheng, S., Zhang, H., Yin, H., Gao, L., Zhang, H., Ma, S., Yang, A., Li, G. *et al.* (2023) Cooperation between NSPc1 and DNA methylation represses HOXA11 expression and promotes apoptosis of trophoblast cells during preeclampsia. *Acta Biochim Biophys Sin (Shanghai)* .33. Guo, W., Zhang, H., Yang, A., Ma, P., Sun, L., Deng, M., Mao, C., Xiong, J., Sun, J., Wang, N. *et al.* (2020) Homocysteine accelerates atherosclerosis by inhibiting scavenger receptor class B member1 via DNMT3b/SP1 pathway. *J Mol Cell Cardiol* , **138** , 34-48.34. Millán-Zambrano, G., Burton, A., Bannister, A.J. and Schneider, R. (2022) Histone posttranslational modifications - cause and consequence of genome function. *Nat Rev Genet* , **23** , 563-580.35. Ma'ayeh, M. and Costantine, M.M. (2020) Prevention of preeclampsia. *Seminars in fetal & neonatal medicine* ,**25** , 101123.36. Rana, S., Lemoine, E., Granger, J.P. and Karumanchi, S.A. (2019) Preeclampsia: Pathophysiology, Challenges, and Perspectives. *Circulation research* , **124** , 1094-1112.37. Nakashima, A., Cheng, S.-B., Ikawa, M., Yoshimori, T., Huber, W.J., Menon, R., Huang, Z., Fierce, J., Padbury, J.F., Sadovsky, Y. *et al.* (2020) Evidence for lysosomal biogenesis proteome defect and impaired autophagy in preeclampsia. *Autophagy* , **16** , 1771-1785.38. Ji, J., Zhou, X., Xu, P., Li, Y., Shi, H., Chen, D., Li, R. and Shi, H. (2019) Deficiency of apoptosis-stimulating protein two of p53 ameliorates acute kidney injury induced by ischemia-reperfusion in mice through upregulation of autophagy. *J Cell Mol Med* ,**23** , 2457-2467.39. Wang, S., Sun, Y., Wang, Y., Wang, A., Kou, B., Che, Y., Chen, D., Zhang, Y. and Shi, Y. (2021) ASPP2 inhibits hepatitis B virus replication by preventing nucleus translocation of HSF1 and attenuating the transactivation of ATG7. *J Cell Mol Med* ,**25** , 6899-6908.40. Hogg, S.J., Beavis, P.A., Dawson, M.A. and Johnstone, R.W. (2020) Targeting the epigenetic regulation of antitumour immunity. *Nat Rev Drug Discov* , **19** , 776-800.41. Zuccarello, D., Sorrentino, U., Brasson, V., Marin, L., Piccolo, C., Capalbo, A., Andrisani, A. and Cassina, M. (2022) Epigenetics of pregnancy: looking beyond the DNA code. *Journal of assisted reproduction and genetics* , **39** , 801-816.42. Chen, Z. and Zhang, Y. (2020) Role of Mammalian DNA Methyltransferases in Development.*Annu Rev Biochem* , **89** , 135-158.43. Kan, R.L., Chen, J. and Sallam, T. (2022) Crosstalk between epitranscriptomic and epigenetic mechanisms in gene regulation. *Trends Genet* , **38** , 182-193.44. Bai, L., Hao, X., Keith, J. and Feng, Y. (2022) DNA Methylation in Regulatory T-Cell Differentiation and Function: Challenges and Opportunities. *Biomolecules* , **12** .45. Navarro-Lafuente, F., Adoamnei, E., Arense-Gonzalo, J.J., Prieto-Sanchez, M.T., Sanchez-Ferrer, M.L., Parrado, A., Fernandez, M.F., Suarez, B., Lopez-Acosta, A., Sanchez-Guillamon, A. *et al.* (2022) Maternal urinary concentrations of bisphenol A during pregnancy are associated with global DNA methylation in cord blood of newborns in the "NELA" birth cohort. *The Science of the total environment* ,**838** , 156540.46. Kassab, A., Gupta, I. and Moustafa, A.A. (2023) Role of E2F transcription factor in oral cancer: Recent insight and advancements. *Seminars in cancer biology* , **92** , 28-41.47. Gao, C., Dong, R., Li, Y., Liang, J. and Tian, H. (2021) MCTS1 promotes the development of lung adenocarcinoma by regulating E2F1 expression.*Oncology letters* , **22** , 531.48. Deng, X., Hua, K., Munankarmy, A., Luo, Q., Wang, X. and Fang, L. (2023) E2F1-mediated ectopic expression of PP1A promotes breast cancer progression via activation of YAP1. *The international journal of biochemistry & cell biology* , **157** , 106389.49. Almacellas, E., Pelletier, J., Manzano, A., Gentilella, A., Ambrosio, S., Mauvezin, C. and Tauler, A. (2019) Phosphofructokinases Axis Controls Glucose-Dependent mTORC1 Activation Driven by E2F1. *iScience* , **20** , 434-448.50. Haim, Y., Bluher, M., Slutsky, N., Goldstein, N., Kloting, N., Harman-Boehm, I., Kirshtein, B., Ginsberg, D., Gericke, M., Guiu Jurado, E. *et al.* (2015) Elevated autophagy gene expression in adipose tissue of obese humans: A potential non-cell-cycle-dependent function of E2F1. *Autophagy* , **11** , 2074-2088.51. Li, Y., Chen, X. and Lu, C. (2021) The interplay between DNA and histone methylation: molecular mechanisms and disease implications. *EMBO Rep* ,**22** , e51803.52. Hashimoto, H., Vertino, P.M. and Cheng, X. (2010) Molecular coupling of DNA methylation and histone methylation.*Epigenomics* , **2** , 657-669.53. Sun, X., Jin, K., Ding, X., Ruan, Z. and Xu, P. (2023) DNA methylation cooperates with H3K9me2 at HCN4 promoter to regulate the differentiation of bone marrow mesenchymal stem cells into pacemaker-like cells. *PLoS One* , **18** , e0289510.54. Xiong, J., Ma, F., Ding, N., Xu, L., Ma, S., Yang, A., Hao, Y., Zhang, H. and Jiang, Y. (2021) miR-195-3p alleviates homocysteine-mediated atherosclerosis by targeting IL-31 through its epigenetics modifications. *Aging Cell*

, **20** , e13485.